doi:10.1038/nature10259

Materials and Methods

Observations

Atmospheric CH_4 mixing ratios have been extensively measured since the late 1970s, and provide valuable information on changes in CH_4 growth rates[1-3]. However, fewer CH_4 stable isotope values, especially δD-CH_4, have been monitored in this time period as compared with its mixing ratio[4-6]. In this study, we constructed recent decadal interhemispheric differences of CH_4 mixing and stable isotopic ratios ($\delta^{13}C$, δD) by using measurements from UCI, NIWA and SIL networks (Table S1). These data were selected because they possessed multiyear δD and $\delta^{13}C$ measurements of atmospheric CH_4 crucial for constraining long-term CH_4 sources and sinks. For each hemisphere we constructed one continuous time series at 40°N and 41°S, using an approach described below in order to study long-term changes in the interhemispheric difference of CH_4 and its isotopes.

The approach of constructing a single time series at mid latitudes in each hemisphere ensured that the $\delta^{13}C$ information was given equal weighting as CH_4 mixing ratio in our budget analysis and inversion calculations. This was crucial for our objective of assessing long-term changes in hemispheric-scale budgets. It is different and complementary from past approaches that have used 3-D atmospheric models to simulate intra-hemispheric as well as interhemispheric CH_4 gradients[7-8] – thus allowing the retrieval of continental-scale variations in sources and sinks. In past applications of the 3-D inversion methodology, the information content from $\delta^{13}C$ was not given equal weighting to mixing ratio observations (that are far more abundant) nor was the

north-south interhemispheric difference (IHD) of $\delta^{13}C$ systematically evaluated as a constraint on long-term changes in the methane budget.

For mixing ratio, data from Niwot Ridge (NWR), Montana de Oro (MDO), Pacific Ocean ship transects sampled between 10–40˚N (POCNH), and remote locations sampled between 30–50˚N (UCI40N) were used to construct the Northern Hemisphere (NH) time series. Baring Head (BHD), Scott Base (AHT), Pacific Ocean ship transects sampled between from 10–40˚S (POCSH) and remote locations sampled between 30–50˚S (UCI40S) were used to construct the Southern Hemisphere (SH) record. Since different primary standards were used in the different networks, an adjustment to mixing ratio data was made to be consistent with the latest National Oceanic and Atmospheric Association (NOAA) CH_4 standard gas scale[9] (NOAA04). For the UCI Tyler network, an adjustment of a factor of 1.0124 to NWR, MDO, and POC (UCI) mixing ratio data was used. The factor is the ratio between NOAA04 (ref. 6) and their previous CH_4 standard gas scale (CMDL83). For the UCI Blake and NIWA network, no adjustment to their mixing ratio presented here was made. It was unnecessary because they use standards traceable to the National Institute for Standards and Technology (NIST) primary standards, and the relative difference between the NOAA04 scale and the NIST CH_4 is only ~0.1% (ref. 9). Fig. 1a shows the original data of mixing ratio in both hemispheres.

For $\delta^{13}C$-CH_4, we used data from the UCI Tyler network (NWR, MDO, and POC) and NIWA network (BHD, AHT, and POC). These two networks have compared standards and flasks, thus minimizing intercalibration issues as described below[5,6,10]. All $\delta^{13}C$ values were reported against an international isotope standard (Vienna Pee Dee belemnite (V-PDB)). The raw data of $\delta^{13}C$-CH_4 are shown in Fig. 1b. For δD-CH_4, data were from UCI Tyler monitored

continental sites (NWR and MDO), and from periodic transects from Tyler and SIL Pacific Ocean cruises (Fig. 1c). $\delta D\text{-}CH_4$ observations were reported versus an established standard: Vienna Standard Mean Ocean Water (V-SMOW).

Details of the sampling procedure and measurement method of CH_4 mixing ratio, $\delta D\text{-}CH_4$ and $\delta^{13}C\text{-}CH_4$ from UCI Tyler network are given by *Tyler et al.* (ref. 11) and *Ajie et al.* (ref. 12). Analyses of CH_4 mixing ratio from UCI Blake network are described by *Simpson et al.* (ref. 13). Descriptions of measurement procedure of CH_4 mixing ratio and $\delta^{13}C\text{-}CH_4$ from NIWA network are reported by *Lowe et al.* (ref. 5). The procedure for the measurement of $\delta D\text{-}CH_4$ from SIL network is documented by *Quay et al.* (ref. 4). Data from the UCI Tyler and UCI Blake network can be accessed through the Carbon Dioxide Information Analysis Center in Oak Ridge, Tennessee (http://cdiac.ornl.gov). The NIWA data are available at ftp://ftp.niwa.co.nz. We also publish new measurements here from the UCI Tyler network for the years 2002-2005.

Removal of the Annual Cycle and Estimation of the Interhemispheric Difference

We removed the annual cycle from the CH_4 and isotope time series using the following approach. First, we fit a 3rd order polynomial through the original data at each site, and removed points greater than 2 standard deviations from the curve. We then averaged all data together within each month to construct a monthly time series. Second, a mean seasonal cycle was constructed by taking an average of all the data within a given month across the multiple years in the time series. Third, we subtracted the mean seasonal cycle from the monthly data. In the exceptional case of Pacific Ocean cruise (POC) data that were more sparsely distributed, we

substituted an annual cycle from MDO in the NH and BHD in the SH. Finally, a monthly mean de-seasonalized time series of the data at each station was constructed (Fig. S6).

As described above, we combined the different sets of observations within each hemisphere to construct a long-term time series. NWR served as the reference site in the NH at 40˚N and BHD served as the reference in the SH at 41˚S. These sites were chosen because NWR had the longest running time series of $\delta^{13}C$ in the NH with measurements from 1989 to 2003 (but with a gap during 1993 and 1994). Similarly, BHD had the longest time series of $\delta^{13}C$ in the SH (for 17 years from 1989 to 2005). Before combining different de-seasonalized data sets, an adjustment was made to each non-reference site within each hemisphere by dividing by a ratio of the site to the corresponding reference site during times when measurements from both sites were available. This was necessary because not all the sites were sampled during the same time period, and because non-reference sites have intra-hemispheric offsets from the reference as a consequence of spatial variability in sources and interactions with atmospheric transport. A single ratio was constructed for each non-reference site from all the months of overlap (Table S1). The year-to-year variation was still a function of the multiple datasets that were available at that time.

In a final step, all of the adjusted time series in each hemisphere were averaged together to form the NH and SH mean time series. For periods of missing data less than six months, we linearly interpolated the gaps. These two series were smoothed using the filtfilt function in Matlab with a 12-month filter window (Fig. 1d-f). The filtfilt function filters the data sequence and generates zero-phase distortion results by processing the input data in both the forward and

reverse directions. The interhemispheric difference (IHD) was defined as the difference between the NH and SH smoothed time series during overlapping time periods (Fig. 1g-i).

Calibration and stability of isotope time series

The isotopic data used for our modelling effort comes primarily from 3 labs (UCI, NIWA, and UW). Of these, two comprised the two longest continuous time series of measurements of atmospheric $\delta^{13}C\text{-}CH_4$ currently available (UCI and NIWA) and had the added advantage of being inter-calibrated through a program by both labs that included comparisons of both individual whole air samples collected by both labs and isotope reference gases used by each lab (which have been calibrated against internationally recognized isotope standards). Most of the $\delta^{13}C\text{-}CH_4$ data was obtained using dual inlet mass spectrometers.

At UCI, there were two types of working isotope reference gases: one was obtained from David Lowe from NIWA, and the other was purchased from Oztech Gas Company (Dallas, Texas. USA). Both reference gases have been intercompared to two internationally recognized CO_2 standards, NBS-19 ($CaCO_3$) and IAEA-CO-9 ($BaCO_3$) (ref. 6). Figure S7 shows the stability of one set of working reference gases (OZ 40 vs. OZ 30) between 1995 and 1999. Another example, Figure S8 shows a similar stability for another working reference gas used between 1999 and 2001. For examples of similar long-term stability in working gases used by the NIWA lab see for example, fig. 3 of *Lowe et al*. (ref. 14) and fig. 1d of *Lowe et al*. (ref. 15). We inter-calibrated with the CH_4 data set of NIWA through an inter-lab comparison during 1995-1999 (ref. 6 and ref. 5). For 16 air samples processed and measured by both laboratories

during 1998-1999 (8 samples from Montaña de Oro and 8 from Baring Head, New Zealand) the agreement for $\delta^{13}C\text{-}CH_4$ was +0.01±0.09‰ (with average values of samples measured at NIWA more enriched by +0.01‰). The methodologies employed by the NIWA lab were described in *Lowe et al*. (ref. 5, 14).

Two-box model

The model we used in this study to examine the mechanisms behind the changes of the interhemispheric differences was based on the Tans two-box model[16]. This model was developed to diagnose responses of the isotopic ratios of atmospheric CH_4 to changes in the source distribution. In the Tans model[16], there are two well-mixed hemispheres with an interhemisperic exchange time (k_T^{-1}) equal to 1.0 year. Sources are generated from both hemispheres, and denoted as S_N and S_S in the Northern Hemisphere (NH) and the Southern Hemisphere (SH), respectively. The CH_4 sink is defined by a decay rate (λ). CH_4 mixing ratios are denoted as M_N and M_S in the NH and the SH, respectively. The equations can be written as:

$$\frac{dM_N}{dt} = S_N - \lambda M_N - k_T M_N + k_T M_S \qquad (1)$$

$$\frac{dM_S}{dt} = S_S - \lambda M_S + k_T M_N - k_T M_S \qquad (2)$$

Similar equations were used to solve for CH_4 isotopes in each hemisphere, with a ^{13}C kinetic isotope effect (KIE, defined as k_{12}/k_{13}). Details of this model have been described by *Tans*[16]. Here, we modified the constant single source input and turnover time in the Tans model[16] with major sources from published literature and a time varying CH_4 lifetime (see *Model simulation scenarios* below for details of model inputs). We also added a module to calculate the hydrogen

isotope (δD) of CH_4 to compare with the observations. The hydrogen KIE (k_h/k_d) for the removal of CH_4 was prescribed as 1.294 (ref. 17). We assumed the ^{13}C KIE associated with the aggregated CH_4 sink was 1.0054. This value was the same as an earlier OH-based estimate[18], but given more recent information suggesting a lower OH-driven ^{13}C KIE of 1.0039 (ref. 17) that is compensated by significant enrichment from strongly fractionating soil and chlorine sinks[19], we believe this value to be a reasonable estimate for the aggregated sink. It is more compatible with low end estimates of the chlorine radical sink[20], but we believe this is justified given remaining uncertainties associated with the chlorine budget. We further examined a range of ^{13}C KIEs (from 1.0039 to 1.0077) in our Monte Carlo simulations. The impacts of these runs are summarized in Table S4.

Comparison with other measurements

We compared the CH_4, $\delta^{13}C$-CH_4 and δD-CH_4 smoothed time series analyzed here with measurements from other independent networks (Fig. S9). For the IHD of CH_4, we inter-compared with two sites operated by NOAA. The two NOAA sites are NWR (40˚N) and CGO (41˚S) from 1983–2005, and can be accessed at ftp://ftp.cmdl.noaa.gov/ccg/. We inter-compared with these two sites because they were the same as (or close to) the locations of our reference sites (NWR and BHD). The IHD of CH_4 reported here agreed reasonably well with observations from NOAA (Fig. S9a), although the decrease in the IHD after 1995 was larger in our time series than in the NOAA observations.

We compared our $\delta^{13}C$-CH_4 IHD time series with measurements from SIL and NOAA networks (Fig. S9b). The SIL sites were OPE (48˚N) and CGO (41˚S) with measurements spanning the period 1988–1996 (SIL data are available at: http://cdiac.ornl.gov). The NOAA

sites in our comparison were NWR and CGO, with measurements publicly available for the 1998–1999 period (NOAA data are available at: ftp://ftp.cmdl.noaa.gov/ccg/). The measured $\delta^{13}C$ IHD reported here during the early 1990s was similar to measurements reported by SIL. For example, during 1989–1993, the $\delta^{13}C$ IHD measured by SIL was -0.31 ± 0.12‰ compared to -0.24 ± 0.11‰ in this study. Comparisons with the NOAA observations did not show the same level of agreement. For the two year period when comparison was possible (1998-1999), the $\delta^{13}C$ IHD measured by NOAA was -0.27 ± 0.10‰ compared to -0.09 ± 0.05‰ in this study.

For $\delta D\text{-}CH_4$, fewer measurements are available for comparison. Data of δD during the cruises made by the SIL network between 1989 and 1996, were comparable to more recent cruise measurements collected between 1997 and 2004 by the UCI Tyler lab (Figs. 1f and 1i). The measurements between these two networks agree well with each other, despite no direct inter-calibration having been made.

Model simulation scenarios

The control simulation (scenario 1), with a time varying CH_4 lifetime (τ), included natural and anthropogenic emissions. The turnover time included components from reaction with OH and stratospheric and soil losses. To include the feedback of CH_4 on tropospheric OH, we assumed the mean lifetime was 9 years in 2005. Then, we estimated the lifetime backward in time as a function of CH_4 by using the following equation described in *Prather et al.* (ref. 21):

$$\frac{\partial \ln(\tau)}{\partial \ln(CH_4)} = 0.28 \qquad (3)$$

This approach assumes that NO_x and CO contributions to OH have approximately balanced each other during the 20th century[21] and thus the primary driver of long-term changes in OH were from atmospheric CH_4. We conducted sensitivity simulations with a fixed 9 year lifetime during the duration of our simulations and obtained quantitatively similar results to those reported in Figures 2b during 1984 through 2005– the period that was the primary focus of our analysis.

We used published CH_4 anthropogenic source histories[22-25], along with a set of constant natural emissions[6,21], to account for decadal variability in global CH_4 source strength from 1700 to 2005. Sources were divided into 9 major categories. The four anthropogenic sources were agricultural sources (rice paddies and animals), landfills, fossil fuels, and biomass burning. The five natural emission sources were tundra, high latitude wetlands (bogs, fens, and lakes), tropical wetlands (swamps, marshes, and seasonally flooded forests), termites, and gas hydrates. Pre-industrial sources at 1700 were prescribed from the work of *Lassey et al.* (ref. 22). To account for the different equilibration time scales for CH_4 and its isotopes[16], we allowed the model to spin-up for 100 years with the constant initial sources. Between 1700 and 1890 (the beginning of the EDGAR-HYDE 1.4 time series) we linearly interpolated emissions between the *Lassey et al.* (ref. 22) and the EDGAR-HYDE 1.4 dataset (http://mnp.nl/edgar/). The EDGAR-HYDE 1.4 dataset is a combination of two time series: the decadal EDGAR-HYDE 1.3 dataset from 1890–1990 (ref. 23) and the EDGAR 3.2 dataset[24] . Briefly, EDGAR-HYDE 1.3 was adjusted to match EDGAR 3.2 estimates for 1970 onwards, to form an inventory with a time step of every ten years during 1890–1970, followed by yearly data through 1995. For the control during 1890 –1980, the EDGAR-HYDE 1.4-based source data was used to drive the model. To create a control in close agreement with the observations before 1980, we adjusted the strength of agricultural sources, including both animal and rice emissions components, to reproduce the Southern

Hemisphere CH_4 and $\delta^{13}C$ observations from 1700 to 1980. These annual adjustments to the agricultural time series were performed once during the construction of the control simulation. They consisted of a scalar adjustment to the total agricultural emissions for each year, leaving the hemispheric percentages of emissions intact as described in Table S3. In subsequent model scenarios and sensitivity tests, we used the same agricultural time series; no further adjustments were made prior to 1980. After 1980, we assumed anthropogenic emission sources remained constant in our control simulation, except for biomass burning emissions. We used Global Fire Emission Database[25] (GFEDv2) to account for the inter-annual variations of fire emissions from 1997 to 2005.

Considering disequilibrium effects on the isotopic composition of methane sources caused by recent trends in atmospheric $\delta^{13}C$-CO_2 (ref. 26), we allowed the carbon isotopic signatures of biogenic sources (high latitude wetlands, tropical wetlands, agricultural sources, biomass burning, and landfills) to change following the trajectories of atmospheric $\delta^{13}C$-CO_2 (refs. 27–28) from 1700 to 2005. We assumed a 5 year turnover time for carbon emitted from wetlands, biomass burning and agricultural sources, and a 10 year turnover time for landfills. Thus, the isotopic signature of these sources became increasingly negative over time as a consequence of increasing inputs of fossil fuel emissions into the atmosphere (and subsequent impacts on isotopic composition of recent photosynthates). Approximate annual strengths of CH_4 emissions, their corresponding carbon and hydrogen isotopic signatures, and the distribution of sources in each hemisphere based on published estimates, are given in Table S3. The anthropogenic and natural sources, and the comparisons between model results and observations, are shown for the control simulation in Fig. S2.

The fossil fuel scenario was identical to the control, except that the magnitude of the NH and SH fluxes associated with fossil fuels were allowed to vary each year after 1980 in order to best match the CH_4 mixing ratio observations in each hemisphere. The agriculture scenario was constructed in an identical way to the fossil fuel scenario, but with isotope ratios for the emissions corresponding to microbial sources instead fossil fuel emissions (Table S3). To reproduce the scenario described in Fig. 2 of *Bousquet et al.* (ref. 8), we generated a simulation (scenario 4) that assumed reductions in CH_4 emissions occurred with a split of 58% fossil fuel emissions and 42% other emissions (including animal, landfill, termite, and ocean fluxes) from the *Bousquet et al*. (ref. 8) study (Fig. S10). This scenario showed a small negative trend of $\delta^{13}C$ IHD that was between the control and fossil fuel simulation (Fig. S10f, Table S2). We also constructed additional sensitivity scenarios with a constant lifetime of CH_4 (described above) and/or without including the disequilibrium effects caused by changes in atmospheric $\delta^{13}C$-CO_2. The sensitivity scenarios include simulations of the control and of fossil fuel and agriculture scenarios. Similar outcomes of these additional scenarios confirmed that the CH_4 slowdown was mainly related to a decrease in agricultural emissions or another isotopically-depleted microbial source. Our findings are supported by one of the inversion scenarios from *Bousquet et al* (ref. 8) that included isotopes (P. Bousquet, personal communication, 2010).

Considering that coal consumption has decreased at a faster pace than natural gas use in several developed countries over the last few decades[29], we constructed two additional scenarios in which the fossil fuel isotopic composition became progressively depleted over the last three decades. Specifically, these runs branched from the control and the fossil fuel scenario to simulate a changing weighted mean $\delta^{13}C$ value associated with coal mining (-37‰) and natural gas leakage (-44‰). In the first fossil fuel trend simulation (scenario 5, Fig. S11), we added a

multi-decadal negative trend in the isotopic composition of the fossil fuel flux- a trend that may be consistent qualitatively with increasing levels of natural gas consumption that have exceeded coal consumption over the past three decades. We assumed there has been a negative trend of 1‰ per decade branching from the control since 1975. This means the control and trend scenarios would be the same prior to 1975, and by 2005, the negative trend scenario would have fossil fuel isotope ratio that is 3‰ lower than the control. Separately, we applied the same negative trend to the fossil fuel scenario (scenario 6, Figs S12). Both trend scenarios showed the temporal variation in fossil fuel isotope ratio did not significantly affect the trends of $\delta^{13}C$ IHD (Table S2, Fig. S11f and Fig. S12f). Nevertheless, both caused an overall depletion of the $\delta^{13}C$ values in both hemispheres (Fig. S11e, Fig. S12e). In addition, we constructed two alternative scenarios by adding a multi-decadal positive trend in the isotopic composition of the fossil fuel flux to simulate more coal had been consumed than natural gas in some developing countries. The outcomes of these alternative scenarios also showed that the trends $\delta^{13}C$ IHD were mostly unaffected by temporal variation in fossil fuel isotope ratio.

Changing rates of methane oxidation

The influence of sink processes on CH_4 slow down, especially the oxidation by the hydroxyl radical (OH) which comprises about 90% of the total sink, is still poorly understood[21]. For example, *Prinn et al*. (ref. 30) used methyl-chloroform (CH_3CCl_3) observations to estimate variations of OH, and derived a positive OH trend in the 1980s followed by an even stronger negative trend during the 1990s. However, *Dreve*t[31] used a 3-D atmospheric chemistry-transport model to examine the OH interannual variation from 1987 to 2005, and suggested that global OH

increased by 8% from 1990 to 1997 followed by a decrease of 5% from 1997 to 2005. This study also suggested that long term trends in OH can not be assessed with CH_3CCl_3 until residual sources, including ocean outgassing, are better constrained[32–33].

In one methane oxidation simulation (scenario 7), we assumed that the global sink processes were solely responsible for the variability in CH_4 growth rate after 1980 (Fig. S13a). In this scenario, we kept the same source history as in the control, but adjusted the loss rate constants in each hemisphere so that modeled mixing ratios matched the observed trajectories. To explain the slowdown, the methane lifetime in the NH would have to decrease from 8.7 years in 1980 to 8.1 years in 2005 (Fig. S13a). In parallel, the methane lifetime in the SH would have to increase by a comparable amount from 8.7 years in 1980 to 9.3 years in 2005. This increase in oxidizing capacity of the NH would correspond to a 0.23 % yr^{-1} increase in OH. The NH trend was close to a past estimate of annual global OH long-term trends (0.2 % yr^{-1}) derived from proxies of CH_3CCl_3 (ref. 34), and slightly lower than an estimate global average OH (0.43 % yr^{-1}) calculated from a 3-D atmospheric chemistry model simulations[35]. We are not aware of any atmospheric chemistry or inversion studies, however, that have provided evidence that the trends in oxidizing capacity between the two hemispheres have diverged. The impact of this scenario on the IHD of $\delta^{13}C$-CH_4 (Fig. S14d) is a reasonable upper bound and accounts for only 20% of the observed trend (Table S2).

In another scenario, we examined the impacts of decreasing OH (-0.20 % yr^{-1}) (Fig. S13b) obtained from a recent OH inversion from 1980–2002 (ref. 8, 36). The decreases in OH scenario (8) could not be constrained by the observed CH_4 and $\delta^{13}C$-CH_4 (Fig. S15a–S15d). In addition, we analyzed the impact of sink scenarios on the trend of δD. The sink scenario (8) with the

recent OH inversion slightly improved the agreement of δD between observed and model results (Fig. S16e, f). Together, these simulations suggest that the changes in the loss processes cannot serve as a primary driver of the CH_4 slow down over the past several decades.

Process-based biogeochemical model

To estimate global CH_4 emissions from rice agriculture during 1960-2005, we modified an empirical process-based model developed by *Huang et al*. (refs. 37–38). The Huang model uses rice net productivity, soil texture, soil temperature, and organic matter amendments to estimate CH_4 flux. This model was applicable to large areas, because it required only few input parameters (such as rice area, yield, growth duration and soil information). In addition, the model has been validated against flooded rice field measurements in various regions, including the United States, China, Indonesia, Philippines, and Italy[37–39].

In this study, we modified the Huang model to account for the impact of chemical fertilizer application and water management practice in rice fields. The use of inorganic fertilizer in rice agriculture has reduced CH_4 emissions per unit of area of rice production[40–42], in part from the displacement of organic amendments that often serve as the carbon substrate for methanogenesis. The practice of intermittent irrigation also can reduce CH_4 emissions by 10–80% as compared with continuous flooding management practices[42–45]. For example, *Jain et al*. (ref. 46) studied the impact of water management on CH_4 fluxes over northern India, and indicated that intermittent irrigation reduces emissions by 20% as compared with continuous flooding management practices. Here, the changes in fertilizer use were estimated using historical fertilizer data sets from the International Rice Research Institute[47] (IRRI). The method

for evaluating the effect of water management was adopted from previous studies[37,44,48,49]. We assumed the practice of intermittent irrigation was widely adopted in Asian countries and linked to the availability of water for agricultural use[44,46,48–51]. We estimated decadal global CH_4 fluxes from 1961 to 2007 using historical rice data sets from IRRI (ref. 47), and field measurements from published literature[38–44,46–51].

Methane budget

In this study, we focused on evaluating the causes for the long-term slowdown of the CH_4 growth rate using the decadal changes in the interhemispheric difference of CH_4 mixing ratio and stable isotope ratio ($\delta^{13}C$ and δD). Using the aforementioned two-box model, we estimated the NH CH_4 flux decreased from 417 ± 10 Tg CH_4 yr^{-1} during 1984–1985 to 386 ± 5 Tg CH_4 yr^{-1} during 2004–2005, while the SH flux remained approximately the same during this same period (starting at 148 ± 5 and ending at 150 ± 5 Tg CH_4 yr^{-1}). These flux estimates, along with CH_4 isotopic signatures, provided useful information to examine changes in CH_4 source and sink processes in each hemisphere over the past three decades. However, owing to these long-term observational records existing almost exclusively in mid-latitude areas, our approach was not intended or designed to resolve CH_4 fluxes from small geographical regions.

Sources of uncertainty

Important sources of uncertainties in our analysis arise from the use of measurements from different networks and incomplete knowledge of the isotopic signatures assigned to individual sources in our model. First, the decadal trend of $\delta^{13}C$-CH_4 was affected by a large

variation during the early 1990s (Fig.1b and 1e). In the NH, a large variation in $\delta^{13}C$ during 1989-1993 was observed by the UCI network. A similar pattern in the SH was also observed by another independent laboratory (the NIWA network). The mechanisms causing the variations in CH_4 during the early 1990s have not been fully resolved[15, 52-54]. Significant changes in $\delta^{13}C$ were not observed at several other stations operated by the SIL network[4] during this time period. However, the SIL multi-year estimate of the IHD of $\delta^{13}C$-CH_4 during this time was of similar magnitude to the UCI/NIWA estimate (e.g., Table S2 and Fig. S9). In this context, its important to note that we combined $\delta^{13}C$ observations from the UCI network and the NIWA network because these two networks have been intercalibrated[5,6,10].

Uncertainty also is introduced from the specification of isotopic source signatures for the individual CH_4 sources in the box model. For example, the isotopic signatures of biogenic sources (e.g. rice paddies, ruminants, and wetlands) span a wide $\delta^{13}C$-CH_4 range from -45 to -76‰ (refs. 6, 55). Most of the thermogenic sources (e.g. natural gas, and coal mining) have values of $\delta^{13}C$-CH_4 between -37 and -44‰ (refs. 6, 56, 57). In our atmospheric analysis using the 2 box model, the rice paddy and animal emissions were combined together as one agriculture source, because we were not able to distinguish the isotopic signatures of rice paddy sources from ruminant emissions. Although reductions in animal emissions cannot be excluded based on our analysis of the atmospheric observations, agricultural statistics suggest that this component of the budget has likely increased in magnitude over the last two decades as a consequence of increased production and consumption of meat in many regions (refs. 23, 24, 58). It is possible, however, that improvements in forage quality for livestock in developed countries may have offset this increasing trend in some regions.

Although natural wetlands have similar isotopic signatures to agricultural sources, there is less evidence that climate or other drivers have modified this source by the amount required to explain the mixing ratio data presented here (Fig. 2a). For example, Walter et al.[59] used a global climate-sensitive process-based methane-hydrology model to study CH_4 emissions from natural wetlands, and found that there was no trend in CH_4 fluxes from wetlands over 1982–1993. Prigent et al.[60] estimated wetlands and surface water areas from 1993–2000 by using satellite observations, and indicated no clear trend in wetlands areas in the NH before 1999. Furthermore, several studies show that changes in environmental conditions (e.g. thawing of permafrost; temperature increases) in high northern latitude regions have probably stimulated CH_4 emissions from wetlands in recent decades[61–63]. We were able to rule out decreases in fossil fuel emissions as a major mechanism for the slowdown, however, because the substantial differences in the isotopic signatures of the biogenic and thermogenic sources had large effects on our model estimates of the IHD of $\delta^{13}C\text{-}CH_4$ (e.g., Figs. 2b).

To evaluate the robustness of our box-model results, we conducted a series of sensitivity and Monte Carlo simulations in which we varied different model parameters, including the inter-hemispheric exchange time, the isotopic fractionation associated with sink processes, and the isotopic signatures of different sources (Table S4). The different sensitivity tests were constructed as follows. In the descriptions and tables below "S" is reserved for primary scenarios used to test hypotheses in the main text and "ST" refers to a sensitivity test in which we modified a single model parameter or conducted Monte Carlo simulations in which parameters were randomly chosen within given ranges.

S-01. Control. The details of the control are described in the previous section of *Model simulation scenarios*.

ST-01. Same as S-01, but the kinetic isotopic fractionation is set as 7.7‰, which is a sink-weighted fractionation factor including non-OH sink processes[19].

ST-02. Monte Carlo Simulation. Same as S-01, but the kinetic isotopic fractionation was randomly selected between 3.9 and 7.7‰ (refs. 17, 19); the $\delta^{13}C\text{-}CH_4$ signature of fossil fuel was randomly selected between -44 and -38‰ (ref. 57); the $\delta^{13}C\text{-}CH_4$ signature of agriculture was randomly selected between -69 and -60‰ (refs. 55, 57); the inter-hemispheric exchange time was randomly selected between 6 and 18 months (ref. 64); this test was conducted 1000 times using a Monte Carlo method.

S-02. Fossil fuel scenario. The settings of this simulation are described in section of *Model simulation scenarios*.

ST-03. Same as S-02, but the kinetic isotopic fractionation related to the OH sink (5.4‰) was replaced by 3.9‰ (ref. 17).

ST-04. Same as S-02, but the kinetic isotopic fractionation related to the OH sink (5.4‰) was replaced by a sink-weighted fractionation factor (7.7‰)(ref. 19).

ST-05. Same as S-02, but the $\delta^{13}C\text{-}CH_4$ signature of fossil fuel was set as -44‰ (ref. 57).

ST-06. Same as S-02, but the inter-hemispheric exchange time was set as 6 months (ref. 64).

ST-07. Same as S-02, but the inter-hemispheric exchange time was set as 18 months (ref. 64).

ST-08. Same as S-02, but the inter-hemispheric exchange time was randomly selected between 6 and 18 months using a Monte Carlo method. This test was conducted 1000 times.

ST-09. Same as S-02, but the $\delta^{13}C\text{-}CH_4$ signature of agriculture was randomly selected between -69 and -60‰ (refs. 55, 57) using a Monte Carlo method. This test was conducted 1000 times.

ST-10. Same as ST-09, but the $\delta^{13}C\text{-}CH_4$ signature of fossil fuel was randomly selected between -44 and -38‰ using a Monte Carlo method. This test was conducted 1000 times.

ST-11. Same as ST-10, but the inter-hemispheric exchange time was randomly selected between 6 and 18 months using a Monte Carlo method. This test was conducted 1000 times.

ST-12. Same as ST-11, but the kinetic isotopic fractionation related to the OH sink (5.4‰) was replaced by a sink-weighted fractionation factor (7.7‰) (ref.19).

ST-13. Same as ST-12, but the kinetic isotopic fractionation was randomly selected between 3.9 and 7.7‰ using a Monte Carlo method. This test was conducted 1000 times.

S-03. Agriculture scenario. The settings of this simulation are described in section of *Model simulation scenarios*.

ST-14. Same as S-03, but the kinetic isotopic fractionation related to the OH sink (5.4‰) was replaced by 3.9‰. (ref. 17).

ST-15. Same as S-03, but the kinetic isotopic fractionation related to the OH sink (5.4‰) was replaced by a sink-weighted fractionation factor (7.7‰)(ref. 19).

ST-16. Same as S-03, but the $\delta^{13}C\text{-}CH_4$ signature of fossil fuel was set as -44‰ (ref. 57).

ST-17. Same as S-03, but the $\delta^{13}C\text{-}CH_4$ signature of agriculture was set as -60‰ (ref. 57).

ST-18. Same as S-03, but the inter-hemispheric exchange time was set as 6 months (ref. 64).

ST-19. Same as S-03, but the inter-hemispheric exchange time was set as 18 months (ref. 64).

ST-20. Same as S-03, but the inter-hemispheric exchange time was randomly selected between 6 and 18 months using a Monte Carlo method. This test was conducted 1000 times.

ST-21. Same as S-03, but the $\delta^{13}C\text{-}CH_4$ signature of fossil fuel was randomly selected between -44 and -38‰ (refs. 6, 57) using a Monte Carlo method. This test was conducted 1000 times.

ST-22. Same as ST-21, but the $\delta^{13}C\text{-}CH_4$ signature of agriculture was randomly selected between -69 and -60‰ using a Monte Carlo method. This test was conducted 1000 times.

ST-23. Same as ST-22, but the inter-hemispheric exchange time was randomly selected between 6 and 18 months using a Monte Carlo method. This test was conducted 1000 times.

ST-24. Same as ST-23, but the kinetic isotopic fractionation related to the OH sink (5.4‰) was replaced by a sink-weighted fractionation factor (7.7‰) (ref.19).

ST-25. Same as ST-24, but the kinetic isotopic fractionation was randomly selected between 3.9 and 7.7‰ using a Monte Carlo method. This test was conducted 1000 times.

References and Notes (Suppl. Inf.)

1. Blake, D. R. & Rowland, F. S. Continuing worldwide increase in tropospheric methane, 1978 to 1987. *Science* **239**, 1129-1131 (1988).

2. Dlugokencky, E. J., Steele, L. P., Lang, P. M. & Masarie, K. A. The growth-rate and distribution of atmospheric methane. *J. Geophys. Res.* **99**, 17021-17043 (1994).

3. Simpson, I. J., Rowland, F. S., Meinardi, S. & Blake, D. R. Influence of biomass burning during recent fluctuations in the slow growth of global tropospheric methane. *Geophys. Res. Lett.* **33**, L22808 (2006).

4. Quay, P. *et al*. The isotopic composition of atmospheric methane. *Global Biogeochem. Cycles* **13**, 445-461 (1999).

5. Lowe, D. C. *et al*. Shipboard determinations of the distribution of C-13 in atmospheric methane in the Pacific. *J. Geophys. Res.* **104**, 26125-26135 (1999).

6. Tyler, S. C., Rice, A. L. & Ajie, H. O. Stable isotope ratios in atmospheric CH_4: Implications for seasonal sources and sinks. *J. Geophys. Res.* **112**, D03303 (2007).

7. Fung, I. *et al*. 3-dimensional model synthesis of the global methane cycle. *J. Geophys. Res.* **96**, 13033-13065 (1991).

8. Bousquet, P. *et al*. Contribution of anthropogenic and natural sources to atmospheric methane variability. *Nature* **443**, 439-443 (2006).

9. Dlugokencky, E. J. *et al*. Conversion of NOAA atmospheric dry air CH_4 mole fractions to a gravimetrically prepared standard scale. *J. Geophys. Res.* **110**, D18306 (2005).

10. Rice, A. L., Gotoh, A. A., Ajie, H. O. & Tyler, S. C. High-precision continuous-flow measurement of $\delta^{13}C$ and δD of atmospheric CH_4. *Anal. Chem.* **73**, 4104-4110 (2001).

11. Tyler, S. C. *et al*. Stable carbon isotopic composition of atmospheric methane: A comparison of surface level and free tropospheric air. *J. Geophys. Res.* **104**, 13895-13910 (1999).

12. Ajie, H. O. *et al*. Measurements and interpretation of surface mixing ratios of CH_4 and CO and $\delta^{13}C$ and δD of CH_4 in air from Pacific Ocean transects between Auckland, New Zealand and Los Angeles, California. *EOS Trans. Amer. Geophys. Union,* **84(46)**, Fall Meet. Suppl., Abstract A52A-0768. 2003.

13. Simpson, I. J., Blake, D. R., Rowland, F. S. & Chen, T. Y. Implications of the recent fluctuations in the growth rate of tropospheric methane. *Geophys. Res. Lett.* **29**, 1479 (2002).

14. Lowe, D. C. *et al*. Concentration and ^{13}C records of atmospheric methane in New Zealand and Antarctica: Evidence for changes in methane sources, *J. Geophys. Res.,* **99(D8)**, 16913–16925 (1994).

15. Lowe, D. C., Manning, M. R., Brailsford, G. W. & Bromley, A. M. The 1991-1992 atmospheric methane anomaly: Southern Hemisphere ^{13}C decrease and growth rate fluctuations. *Geophys. Res. Lett*. **24**, 857-860 (1997).

16. Tans, P. P. A note on isotopic ratios and the global atmospheric methane budget. *Global Biogeochem. Cycles* **11**, 77-81 (1997).

17. Saueressig, G. *et al*. Carbon 13 and D kinetic isotope effects in the reactions of CH_4 with O(1D) and OH: New laboratory measurements and their implications for the isotopic composition of stratospheric methane. *J. Geophys. Res*., **106(19)**, 23127-23138. (2001).

18. Cantrell, C. A. *et al*. Carbon kinetic isotope effect in the oxidation of methane by the hydroxyl radical. *J. Geophys. Res.* **95**, 22455-22462 (1990).

19. Lassey, K. R., Etheridge, D. M., Lowe, D. C., Smith, A. M. & Ferretti, D. F. Centennial evolution of the atmospheric methane budget: What do the carbon isotopes tell us? *Atmos. Chem. Phys.* **7**, 2119–2139 (2007).

20. Allan, W., H. Struthers, H. & Lowe, D. C. Methane carbon isotope effects caused by atomic chlorine in the marine boundary layer: Global model results compared with Southern Hemisphere measurements, *J. Geophys. Res*., **112**, D04306, doi:10.1029/2006JD007369 (2007).

21. Prather, M. *et al*. in *Climate Change 2001: The Scientific Basis* (eds. Houghton J. T. *et al*.) 241–287 (Cambridge Univ. Press, New York, 2001).

22. Lassey, K. R., Lowe, D. C. & Manning, M. R. The trend in atmospheric methane $\delta^{13}C$ implications for isotopic constraints on the global methane budget. *Global Biogeochem. Cycles* **14**, 41-49 (2000).

23. van Aardenne, J. A., Dentener, F. J., Olivier, J. G. J., Goldewijk, C. G. M. K. & Lelieveld, J. A 1 degrees x 1 degrees resolution data set of historical anthropogenic trace gas emissions for the period 1890-1990. *Global Biogeochem. Cycles* **15**, 909-928 (2001).

24. Olivier, J. G. J. & Berdowski, J. J. M. in *The Climate System: Global emissions sources and sinks*. (eds. Berdowski, J., Guicherit, R. & B.J. Heij) 33-78. (A.A. Balkema Publishers/Swets & Zeitlinger Publishers, Lisse, The Netherlands, 2001).

25. van der Werf, G. R. *et al*. Interannual variability in global biomass burning emissions from 1997 to 2004. *Atmospheric Chemistry and Physics* **6**, 3423-3441 (2006).

26. Schaefer, H. & Whiticar, M. J. Potential glacial-interglacial changes in stable carbon isotope ratios of methane sources and sink fractionation. *Global Biogeochem. Cycles* **22**, GB1001, doi: 1010.1029/2006GL002889 (2008).

27. Francey, R. J. *et al.* A 1000-year high precision record of $\delta^{13}C$ in atmospheric CO_2. *Tellus*, **51B (2)**: 170-193 (1999).

28. *Monthly $\delta^{13}C$-CO_2 from Manua Loa station*. <ftp://ftp.cmdl.noaa.gov/ccg/co2c13/flask/month/> (National Oceanic and Atmospheric Association; 2009, accessed 12 December 2009)

29. *Global Anthropogenic Non-CO_2 Greenhouse Gas Emissions: 1990–2020* <http://www.epa.gov/climatechange/economics/downloads/GlobalAnthroEmissionsReport.pdf> (United States Environmental Protection Agency, 2006)

30. Prinn, R. G. *et al*. Evidence for substantial variations of atmospheric hydroxyl radicals in the past two decades. *Science* **292**, 1882-1888 (2001).

31. Drevet, J. Modeling study of the interannual variability in global tropospheric hydroxyl radical and methane concentrations over the last two decades. Ph.D. dissertation, Ecole Polytechnique Federale de Lausanne, Suisse. (2008).

32. Krol, M. & Lelieveld, J. Can the variability in tropospheric OH be deduced from measurements of 1,1,1-trichloroethane (methyl chloroform)? *J. Geophys. Res.* **108**, 4125 (2003).

33. Wennberg, P. O., Peacock, S., Randerson, J. T. & Bleck, R. Recent changes in the air-sea gas exchange of methyl chloroform. *Geophys. Res. Lett.* **31**, L16112 (2004).

34. Prinn, R. G. *et al*. Evidence for variability of atmospheric hydroxyl radicals over the past quarter century. *Geophys. Res. Lett.* **32**, L07809 (2005).

35. Karlsdottir, S. & Isaksen, I. S. A. Changing methane lifetime: Possible cause for reduced growth. *Geophys. Res. Lett.* **27**, 93-96 (2000).

36. Bousquet, P., Hauglustaine, D. A., Peylin, P., Carouge, C. & Ciais, P. Two decades of OH variability as inferred by an inversion of atmospheric transport and chemistry of methyl chloroform. *Atmos Chem Phys*. **5**, 2635-2656 (2005).

37. Huang, Y., Sass, R. L. & Fisher, F. M. Model estimates of methane emission from irrigated rice cultivation of China. *Global Change Biol*. **4**, 809-821 (1998).

38. Huang, Y., Sass, R. L. & Fisher, F. M. A semi-empirical model of methane emission from flooded rice paddy soils. *Global Change Biol*. **4**, 247-268 (1998).

39. Sass, R. L., Fisher, F. M. & Huang, Y. A process-based model for methane emissions from irrigated rice fields: experimental basis and assumptions. *Nutrient Cyc. Agroecosyst*. **58**, 249-258 (2000).

40. Minami, K. Methane from rice production. *Fert. Res*. **37**, 167-179. (1994).

41. Wassmann, R. *et al*. Fluxes and pools of methane in wetland rice soils with varying organic inputs. *Environ. Monit. Assess*. **42**, 163-173 (1996).

42. Wassmann, R. *et al*. Characterization of methane emissions from rice fields in Asia: III. Mitigation options and future research needs. *Nutr. Cycl. Agroecosyst.* **58**, 23–36 (2000).

43. Sass, R. L., Fisher, F. M., Wang, Y. B., Turner, F. T. & Jund, M. F. Methane emission from rice fields: The effect of floodwater management. *Global Biogeochem Cycles* **6**, 249–262 (1992).

44. Li, C. S. *et al*. Reduced methane emissions from large-scale changes in water management of China's rice paddies during 1980-2000. *Geophys. Res. Lett.* **29**, 1972 (2002).

45. Frolking, S., Li, C. S., Braswell, R. & Fuglestvedt, J. Short- and long-term greenhouse gas and radiative forcing impacts of changing water management in Asian rice paddies. *Global Change Biol.* **10**, 1180-1196 (2004).

46. Jain, M. C. *et al*. Methane emissions from irrigated rice fields in northern India (New Delhi). *Nutr. Cycling Agroecosyst.* **58**, 75-83 (2000).

47. *World Rice Statistics* <http://irri.org/world-rice-statistics> (International Rice Research Institute, 2008; accessed 22 September 2008).

48. Kai, F. M. Assessing causes of global methane changes during 1979-2007 using measurements and models of mixing ratios and stable isotopes. Ph.D. dissertation, Univ. of California at Irvine, Irvine. (2009).

49. Kai, F. M., Tyler, S. C. & Randerson, J. T. Modeling methane emissions from rice agriculture in China during 1961-2007. *Journal of Integrative Environmental Sciences* **7:2**, 49–60 (2010).

50. Yagi, K., Tsuruta, H., Kanda, K. & Minami, K. Effect of water management on methane emission from a Japanese rice paddy field: Automated methane monitoring, *Global Biogeochem Cycles* **10**, 255–267 (1996).

51. Cai, Z. C. A category for estimate of CH_4 emission from rice paddy fields in China, *Nutr. Cycl. Agroecosys*. **49**, 171-179 (1997).

52. Bekki, S., Law, K. S. & Pyle, J. A. Effect of ozone depletion on atmospheric CH_4 and CO concentrations. *Nature* **371**, 595-597 (1994).

53. Dlugokencky, E. J. *et al*. A dramatic decrease in the growth-rate of atmospheric methane in the northern-hemisphere during 1992. *Geophys. Res. Lett.* **21**, 45-48 (1994).

54. Gupta, M., Tyler, S. & Cicerone, R. Modeling atmospheric $\delta^{13}C$-CH_4 and the causes of recent changes in atmospheric CH_4 amounts. *Journal of Geophysical Research-Atmospheres* **101**, 22923-22932 (1996).

55. Cicerone, R. J., & Oremland, R. S. Biogeochemical aspects of atmospheric methane, *Global Biogeochem. Cycles* **2**, 299-327 (1988).

56. Whiticar, M. & Schaefer, H. Constraining past global tropospheric methane budgets with carbon and hydrogen isotope ratios in ice. *Philosophical Transactions of the Royal Society A-Mathematical Physical and Engineering Sciences* **365**, 1793-1828 (2007).

57. Mikaloff Fletcher, S. E., Tans, P. P., Bruhwiler, L. M., Miller, J. B. & Heimann, M. CH_4 sources estimated from atmospheric observations of CH_4 and its C-13/C-12 isotopic ratios: 1. Inverse modeling of source processes. *Global Biogeochem. Cycles* **18**, GB4004 (2004).

58. Verge, X., de Kimpe, C. & Desjardins, R. Agricultural production, greenhouse gas emissions and mitigation potential. *Agric. Forest Meteorol.* **142**, 255–269 (2007).

59. Walter, B. P., Heinman, M., & Matthews, E. Modeling modern methane emission from natural wetlands: 2. Interannual variations 1982–1993, *J. Geophys. Res*., **106**, 34,207 – 34,219. (2001).

60. Prigent, C., Papa, F., Aires, F., Rossow, W. B. & Matthews, E. Global inundation dynamics inferred from multiple satellite observations, 1993-2000. *J. Geophys. Res.* **112**, D12107 (2007).

61. Johansson, T. *et al*. Decadal vegetation changes in a northern peatland, greenhouse gas fluxes and net radiative forcing. *Global Change Biol.* **12**, 2352-2369 (2006).

62. Zhuang, Q. *et al*., Methane fluxes between terrestrial ecosystems and the atmosphere at northern high latitudes during the past century: A retrospective analysis with a process-based biogeochemistry model*, Global Biogeochem. Cycles*, **18**, GB3010 (2004).

63. Bloom, A. A., Palmer, P. I., Fraser A., Reay D. & Frankenberg C. Large-scale controls of methanogenesis inferred from methane and gravity spaceborne data. *Science*. **327**, 322-325, (2010).

64. Bowman K. P. & Cohen, P. J. Interhemispheric exchange by seasonal modulation of the Hadley circulation. *Journal of the Atmospheric Sciences* **54(16)**, 2045-2059 (1997).

65. Bergamaschi, P. *et al*. Transects of atmospheric CO, CH_4, and their isotopic composition across the Pacific: Shipboard measurements and validation of inverse models. *J. Geophys. Res.* **106**, 7993-8011 (2001).

66. Stevens, C. M. & Wahlen, M. in *Atmospheric Methane: Its Role in the Global Environment,* The isotopic composition of atmospheric methane and its sources (ed, Khalil, M. A. K) 25-41 (Springer, New York, 2000).

67. Matsumoto, R. *et al*. in *Proc. ODP, Sci. Results, 164*: College Station, TX (Ocean Drilling Program), Occurrence, structure, and composition of natural gas hydrate recovered from the Blake Ridge, northwest Atlantic. (eds. Paull, C. K., Matsumoto, R., Wallace, P. J. & Dillon, W. P.) 13–28. doi:10.2973/odp.proc.sr.164.247.(2000).

68. Randerson, J. T. *et al*. Fire emissions from C-3 and C-4 vegetation and their influence on interannual variability of atmospheric CO_2 and $\delta^{13}C$-CO_2. *Global Biogeochem. Cycles* **19**, GB2019 (2005).

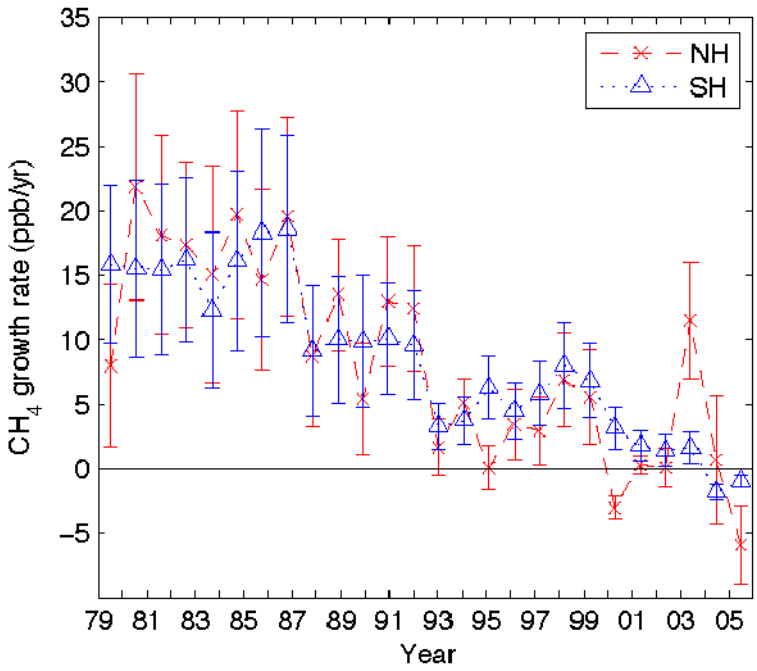

Figure S1. Interannual variations in the CH_4 growth rate from 1979 to 2005 in the NH and SH. These curves were the derivative with respect to time of the smoothed trend from Fig. 1d. Error bars are 1 s.d. of the calculated growth rates.

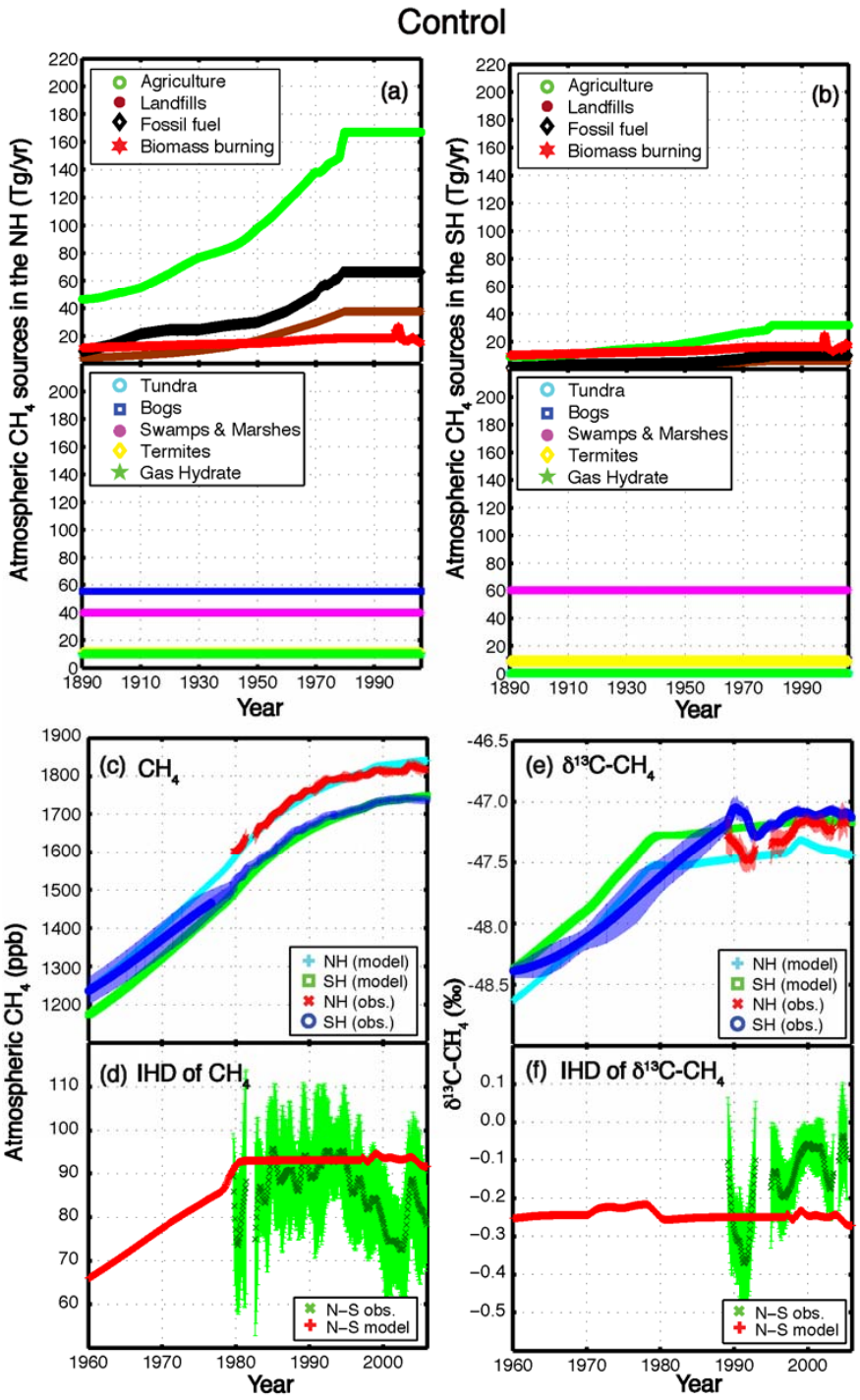

Figure S2. Model input fluxes and model-data comparisons for the control simulation (scenario 1). The model source inputs for the control run (**a, b**) were the EDGAR-HYDE 1.4-based anthropogenic source history and the constant natural sources summarized in Table S3. Observed CH_4 mixing ratio and $\delta^{13}C$-CH_4 in the NH and the SH, as well as the interhemispheric differences (IHD), are compared with model results (**c** to **f**). Error bars are 1 standard deviation (s.d.) based on all the adjusted observations in a 12-month window centred at each monthly time step.

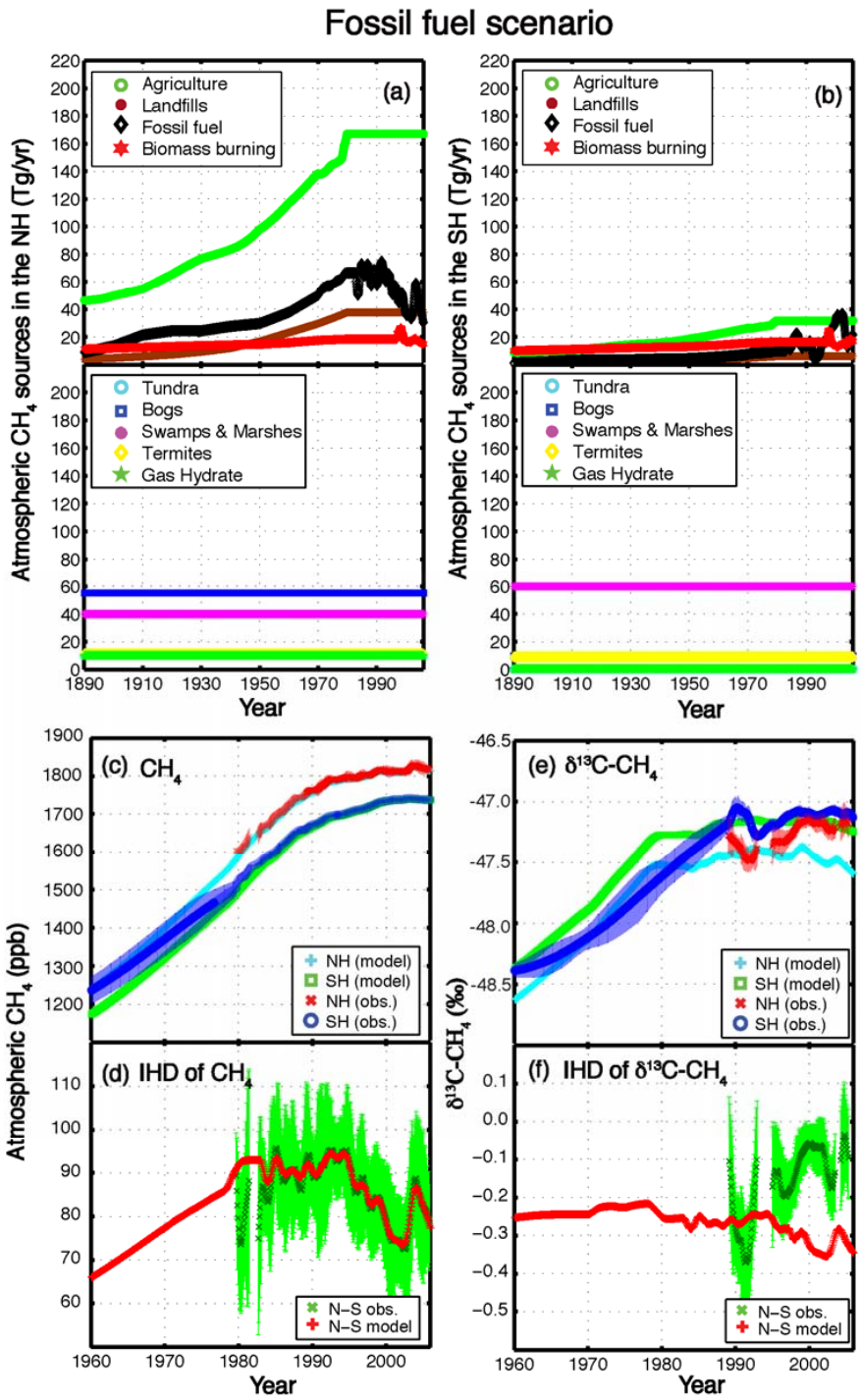

Figure S3. Model results from the fossil fuel simulation (scenario 2). In this scenario we modified only fossil fuel emissions (**a, b**) to test whether the decreases in fossil fuel were solely responsible for the CH_4 slow down. As expected, the model reproduces the observed CH_4 mixing ratio (**c**) and IHD of CH_4 (**d**). This scenario, however, could not capture the variations of $\delta^{13}C\text{-}CH_4$ (**e**) and shows a widening of the IHD of $\delta^{13}C\text{-}CH_4$, the opposite of that observed (**f**). Error bars are 1 standard deviation (s.d.) based on all the adjusted observations in a 12-month window centred at each monthly time step.

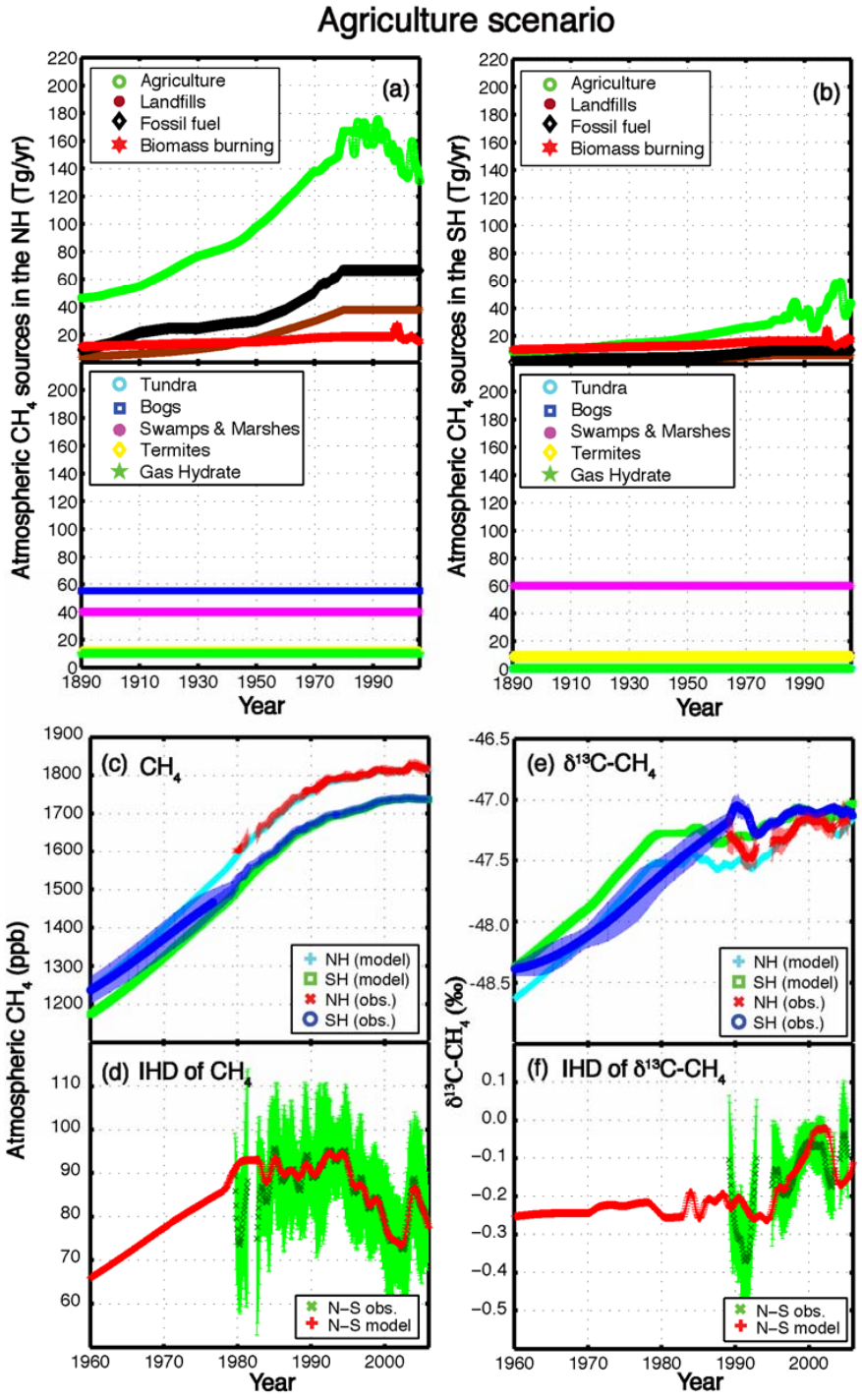

Figure S4. Model results from the agriculture simulation (scenario 3). This scenario examines the role of decreasing agricultural sources as the primary driver of the CH_4 slow down, by solely adjusting the agricultural flux term to match recent variations in mixing ratio (**a, b**). As expected, like scenario 2, the model reproduces the CH_4 mixing ratio measurements (**c**) and the IHD of CH_4 (**d**). This scenario, however, shows substantial improvements in the agreement between

model and observations of $\delta^{13}C\text{-}CH_4$ (**e, f**) and the IHD of $\delta^{13}C\text{-}CH_4$ (**f**). This implies that reductions in an isotopically depleted source in the NH, such as decreased emissions from rice agriculture, contributed substantially to the CH_4 slow down. Error bars are 1 standard deviation (s.d.) based on all the adjusted observations in a 12-month window centred at each monthly time step.

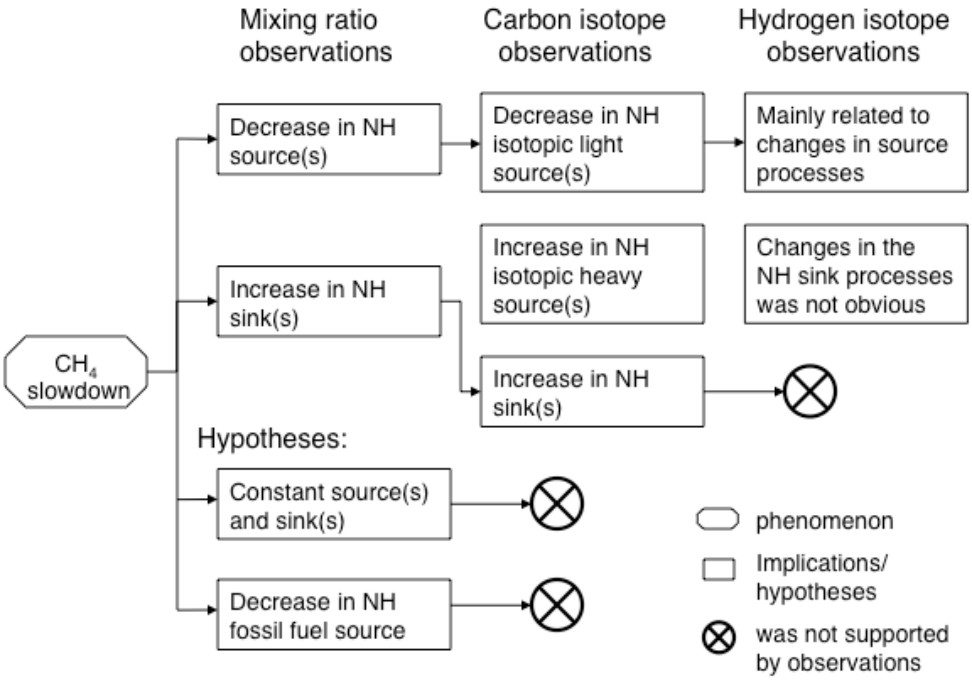

Figure S5. A schematic of main findings of CH_4 mixing ratio and isotopic data analyses. Major findings, implications and hypotheses related to different dataset are described and evaluated in each column from left to right.

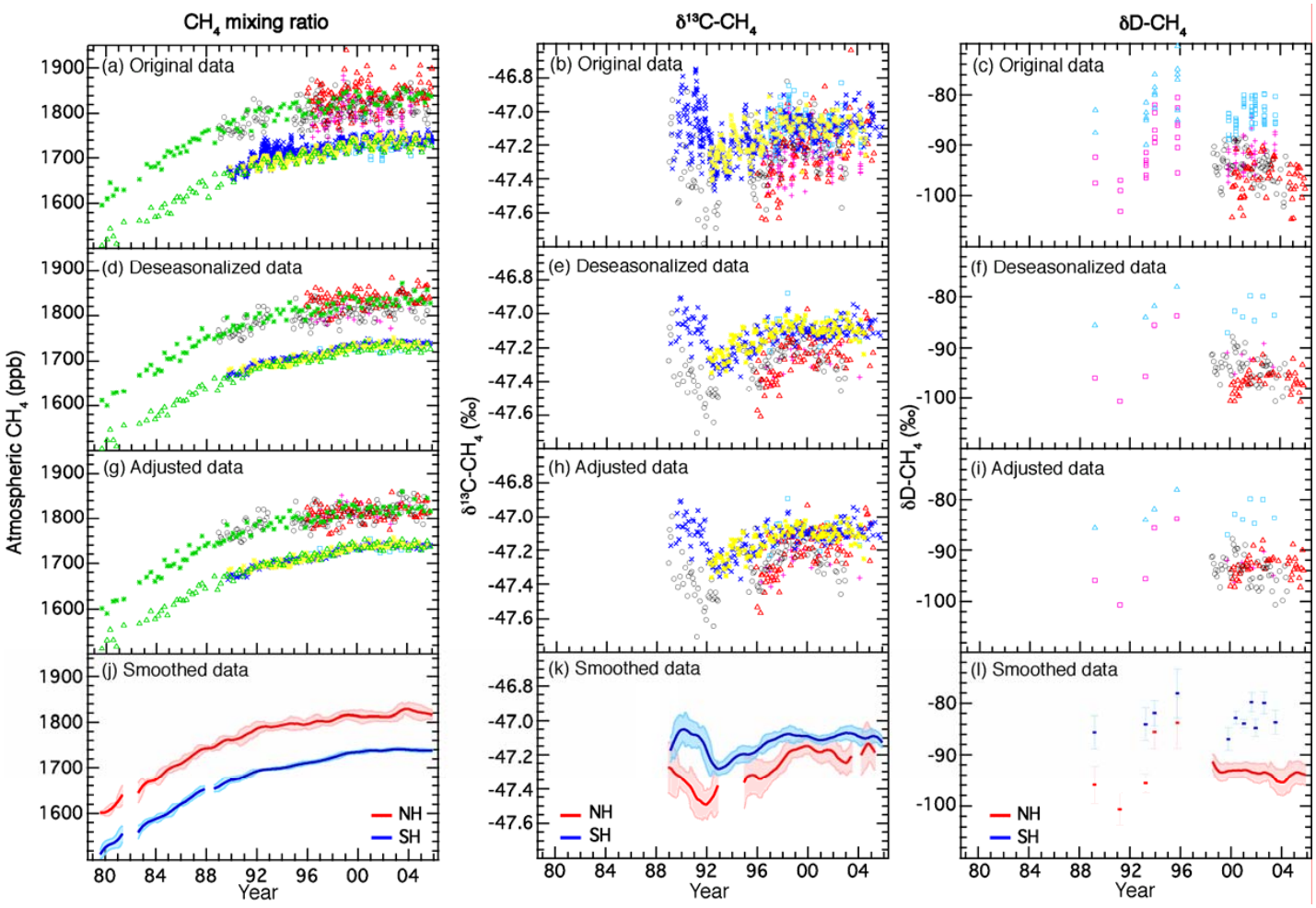

Figure S6. Approach for constructing the NH and SH time series of atmospheric CH_4, $\delta^{13}C$-CH_4, and δD-CH_4. (**a** to **c**) Original measurements used in our analysis. The observing stations are NWR (black circles), MDO (red triangles), POCNH (magenta pluses), UCI40N (green asterisks), SIL-POCNH (magenta squares), BHD (blue crosses), AHT (yellow asterisks), POCSH (cyan squares), UCI40S (green triangles), SIL-POCSH (cyan triangles). (**d** to **f**) Deseasonalized monthly mean measurements of at individual sites. We obtained these data after removing outliers (points greater 2 s.d.) and the mean seasonal cycle from each site. (**g** to **i**) Adjusted monthly mean observations at individual sites. To reduce the influence of intra-hemispheric variability from heterogeneous source distributions, a single scalar was applied to each deseasonalized time series within each hemisphere to improve agreement with the reference time series (Table S1). (**j** to **l**) 12-month smoothed trends in CH_4, $\delta^{13}C$-CH_4, and δD-CH_4 between the NH (red line) and SH (blue line) time series. Error bars are 1 s.d. based on all the adjusted

observations in a 12-month window centered at each monthly time step. For δD-CH_4, the error bars are 1 s.d. of the calculated monthly trends for the Pacific voyage measurements.

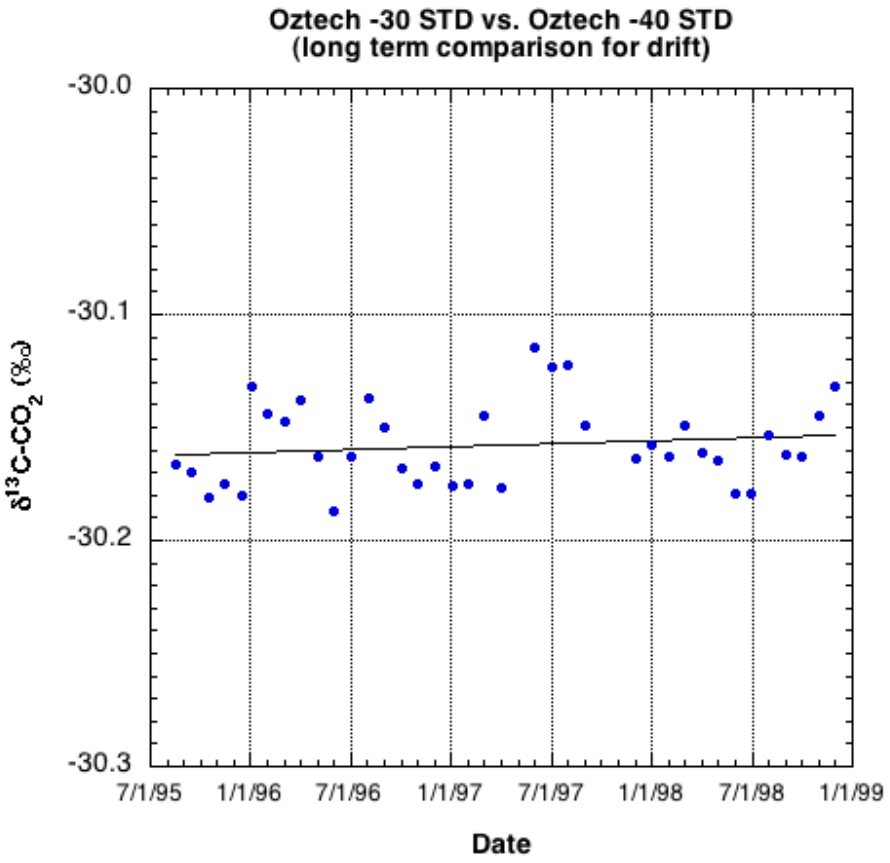

Figure S7. The stability of primary standard for δ^{13}C-CH_4 between 1995 and 1999. The long term comparison between two synthetic air standards (OZ 40 and OZ 30) shows the drift of the standard was very small.

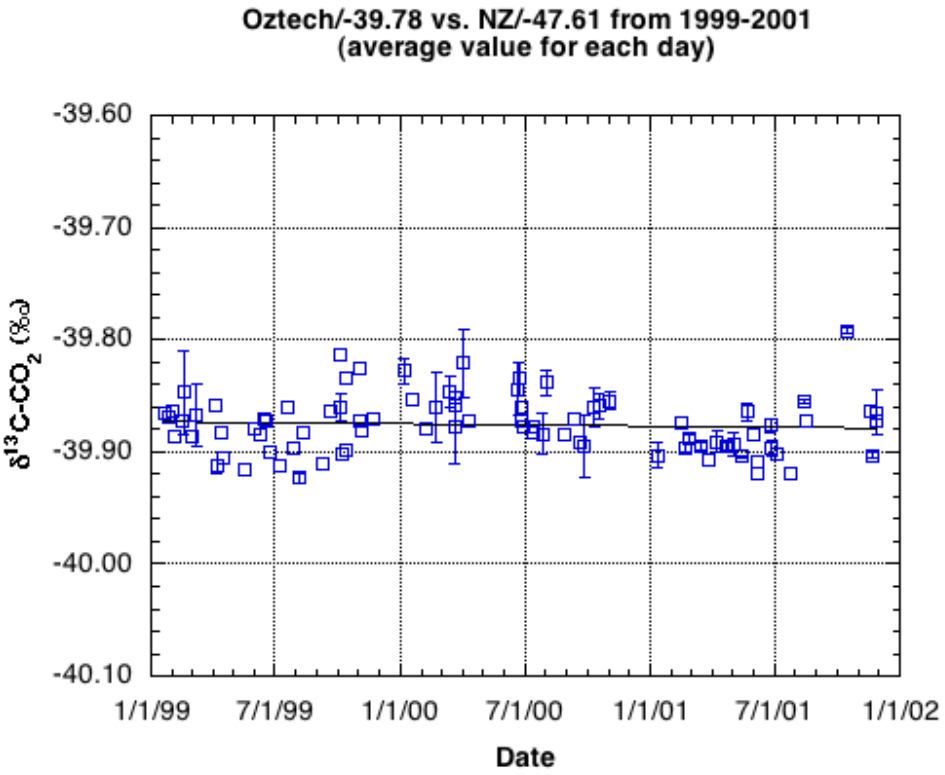

Figure S8. The stability of primary standards for δ^{13}C-CH_4 between 1999 and 2001. The comparison between two synthetic air standards (OZ 40 and NZ 48) shows the main reference gas for δ^{13}C-CH_4 was considerable stable during these time periods. Error bars are 1 standard deviation (s.d.) of the mean of measurements.

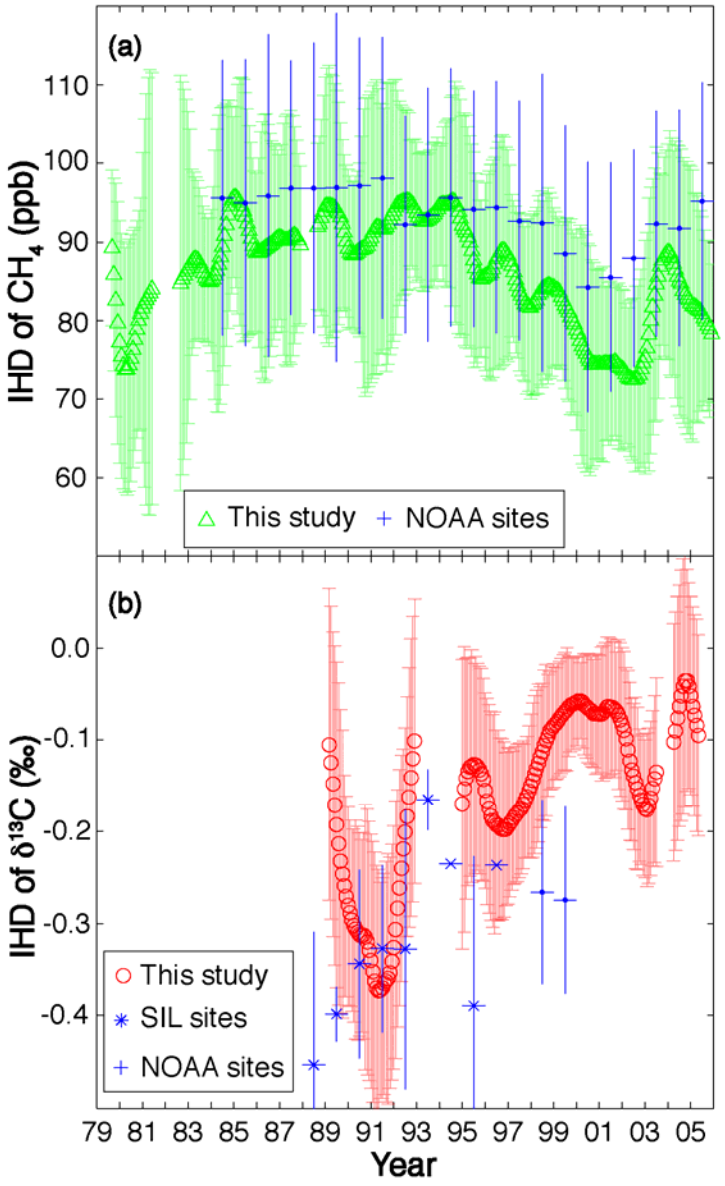

Figure S9. Comparison of observations between this study and other networks. (**a**) Comparison of interhermispheric differences of in CH_4 between this study and the NOAA network. (**b**) Comparison of interhermispheric differences of $\delta^{13}C$-CH_4 between this study and the SIL and NOAA networks. Error bars are 1 s.d. based on all the adjusted observations in a 12-month moving window. For NOAA and SIL sites, error bars are 1 s.d. of the calculated annual means for CH_4 and $\delta^{13}C$-CH_4.

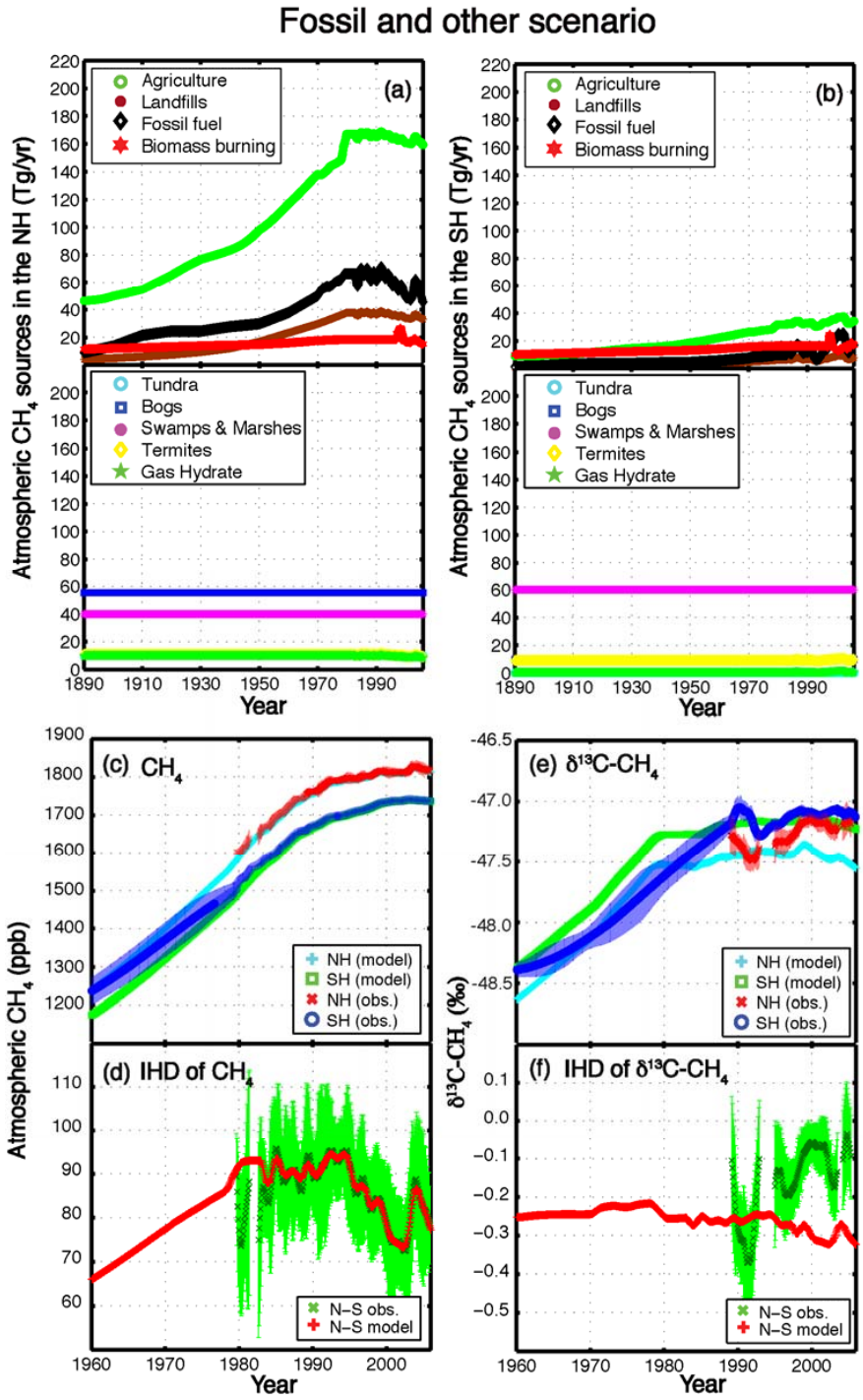

Fig. S10. Model results from the fossil fuel and others scenario from *Bousquet et al*. (ref. 8) (scenario 4). This scenario was designed to reproduce the previous findings[8,9] that a decrease in NH anthropogenic source was partly responsible for the CH_4 slowdown during the 1990s. This simulation assumes the CH_4 slowdown was caused by decreases in NH fossil fuel and other emissions during that time period (**a**). The model matches the CH_4 mixing ratio measurements (**c**) and the IHD of CH_4 (**d**). However, this scenario did not improve agreement of the $\delta^{13}C$ IHD between model and observed results (**f**). Error bars are 1 standard deviation (s.d.) based on all the adjusted observations in a 12-month window centred at each monthly time step.

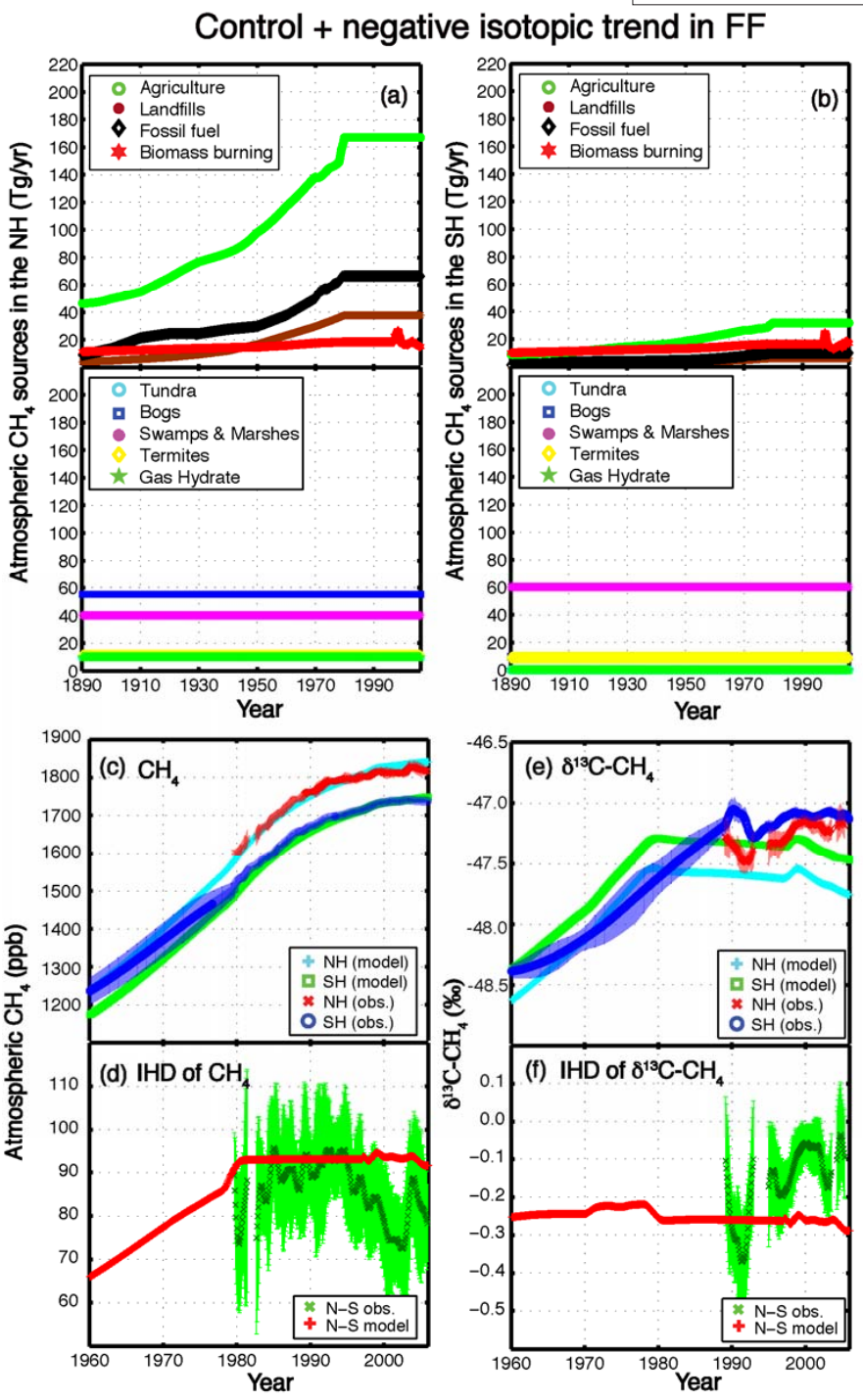

Figure S11. Model results from the control plus a negative isotopic trend in fossil fuel emissions (scenario 5). This scenario tests the influence of temporal variations in fossil fuel isotope ratio, by adding a multi-decadal negative trend in the isotopic composition of the fossil fuel flux after 1975 branching from the control. Like the control, this scenario captured the long-term trends in observed CH_4 mixing ratio (**a**) and IHD of CH_4 (**b**). This negative trend scenario show the overall $\delta^{13}C$ values in both hemispheres would become more depleted (negative) (**e**) because of the changes in fossil fuel isotope ratio, however, the trend of $\delta^{13}C$ IHD remained about the same

compared to the control (**f**). Error bars are 1 standard deviation (s.d.) based on all the adjusted observations in a 12-month window centred at each monthly time step.

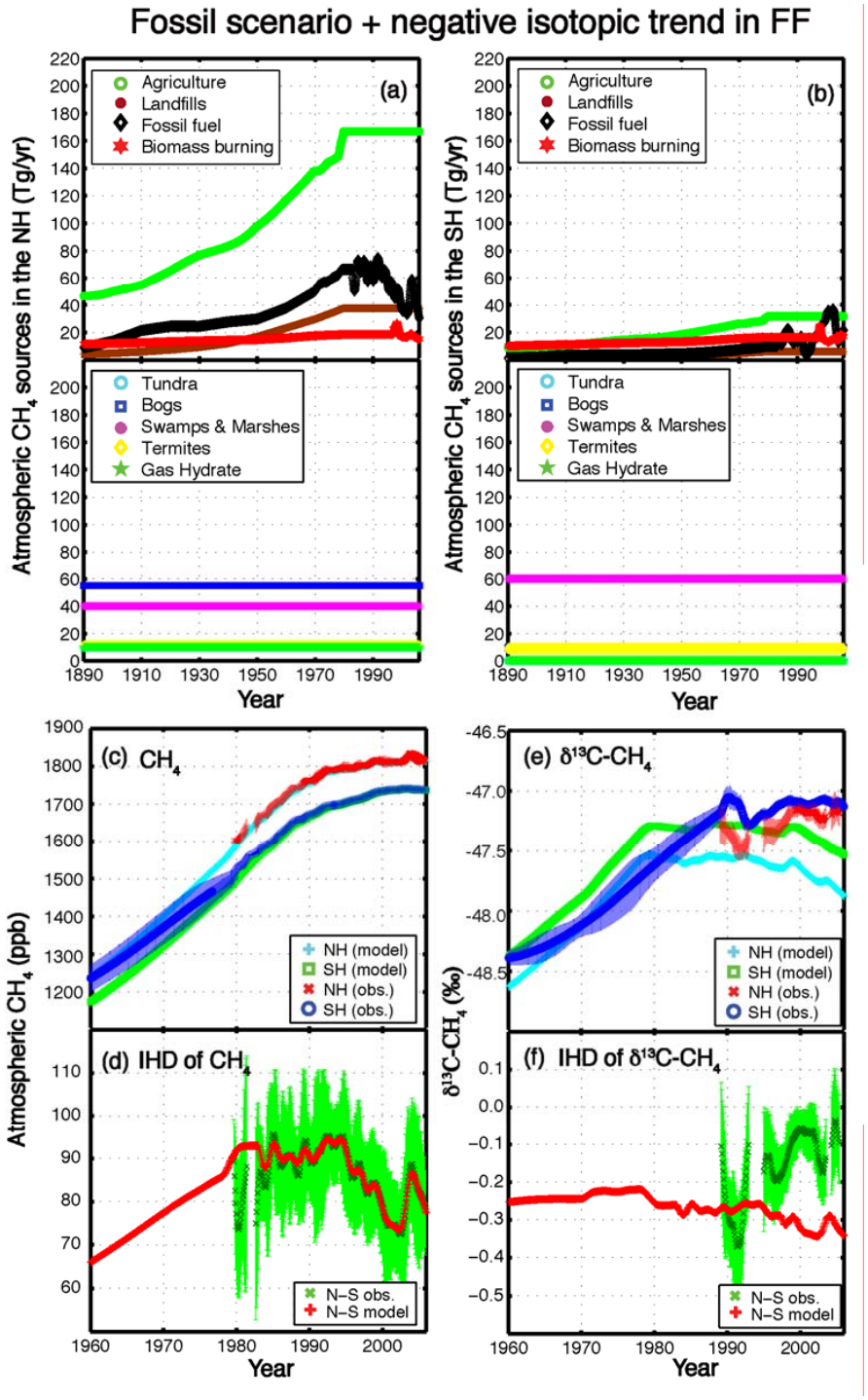

Figure S12. Model results from the fossil scenario plus a negative isotopic trend in fossil fuel emissions (scenario 6). This scenario appended a multi-decadal negative trend to the isotopic composition of the fossil fuel flux branching from the fossil scenario. Like scenario 5, this

negative trend scenario has little impact on the trend of $\delta^{13}C$ IHD (**f**), and, the overall $\delta^{13}C$ values will become more depleted (negative) (**e**) if natural gas has slowly replaced coal as the primary fossil CH_4 source. Error bars are 1 standard deviation (s.d.) based on all the adjusted observations in a 12-month window centred at each monthly time step.

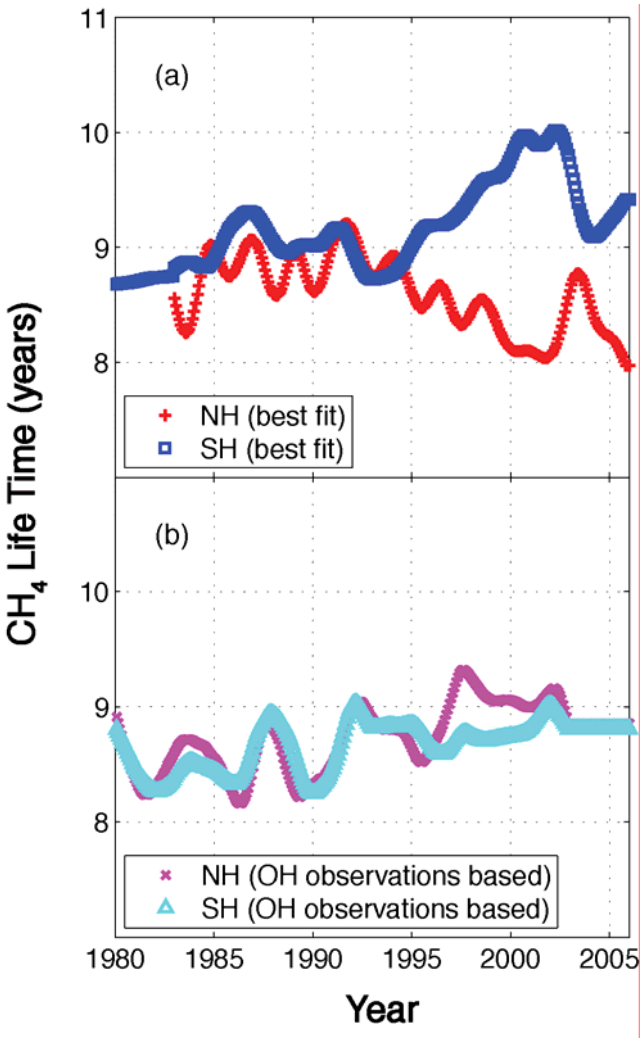

Fig. S13. Estimates of CH_4 lifetimes during 1980-2005. (**a**) The CH_4 lifetimes were deduced by adjusting the lifetimes of CH_4 to best fit CH_4 mixing ratio observations. The increase in oxidizing capacity of the NH would correspond to a 0.23% yr^{-1} increase in OH during 1980–2005. (**b**) The trends of CH_4 lifetimes were derived from recent OH inversion from 1980–2002 (ref. 8, 36), which show a decreasing OH trend (-0.20% yr^{-1}) in the NH.

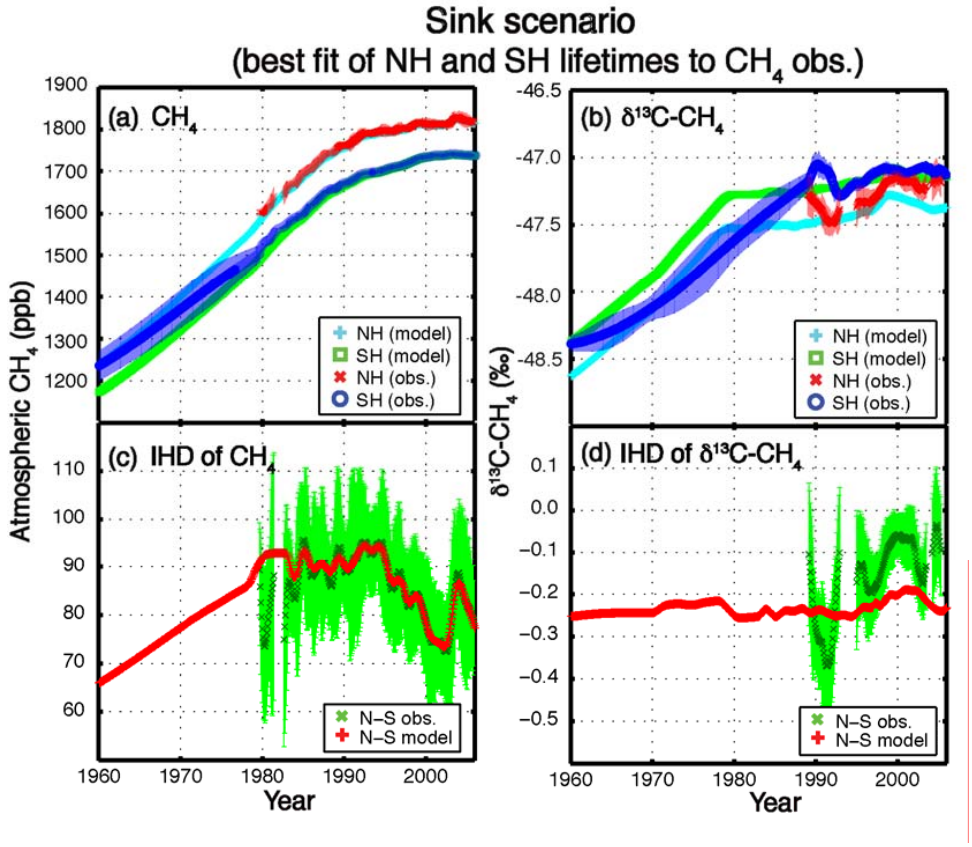

Fig. S14. Model results for the changing sink simulation (scenario 7). This scenario examines possible changes in sink processes by adjusting the loss rate of CH_4 (instead of sources) to reproduce mixing ratio observations. As with scenarios 2 and 3, the model with the best fit lifetimes (see Fig. S13a) reproduced the CH_4 mixing ratio measurements (**a**) and the IHD of CH_4 (**c**). Impacts on the IHD of $\delta^{13}C$-CH_4 (**d**) were in the right direction as the observations but smaller than the other scenarios in which the agricultural source term was adjusted. Error bars are 1 standard deviation (s.d.) based on all the adjusted observations in a 12-month window centred at each monthly time step.

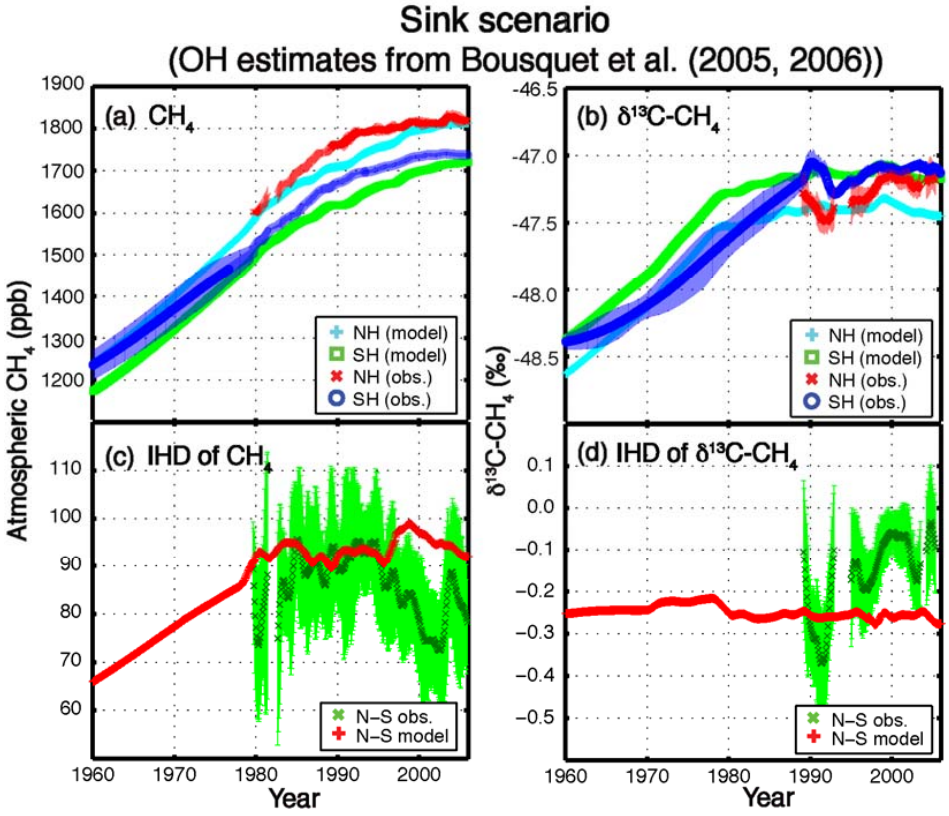

Fig. S15. Model results for a sink simulation using a recent OH inversion lifetime (scenario 8). This scenario applied a deduced liftetime trend obtained from a recent OH inversion (ref. 8, 36, see Fig. S13b) to test the influence of contemporary variability of OH on CH_4 mixing and isotope ratios. The model does not match the CH_4 mixing ratio (**a**, **c**) or $\delta^{13}C$-CH_4 measurements (**b**, **d**), implying that a change in sources is required to close the budget. Error bars are 1 standard deviation (s.d.) based on all the adjusted observations in a 12-month window centred at each monthly time step.

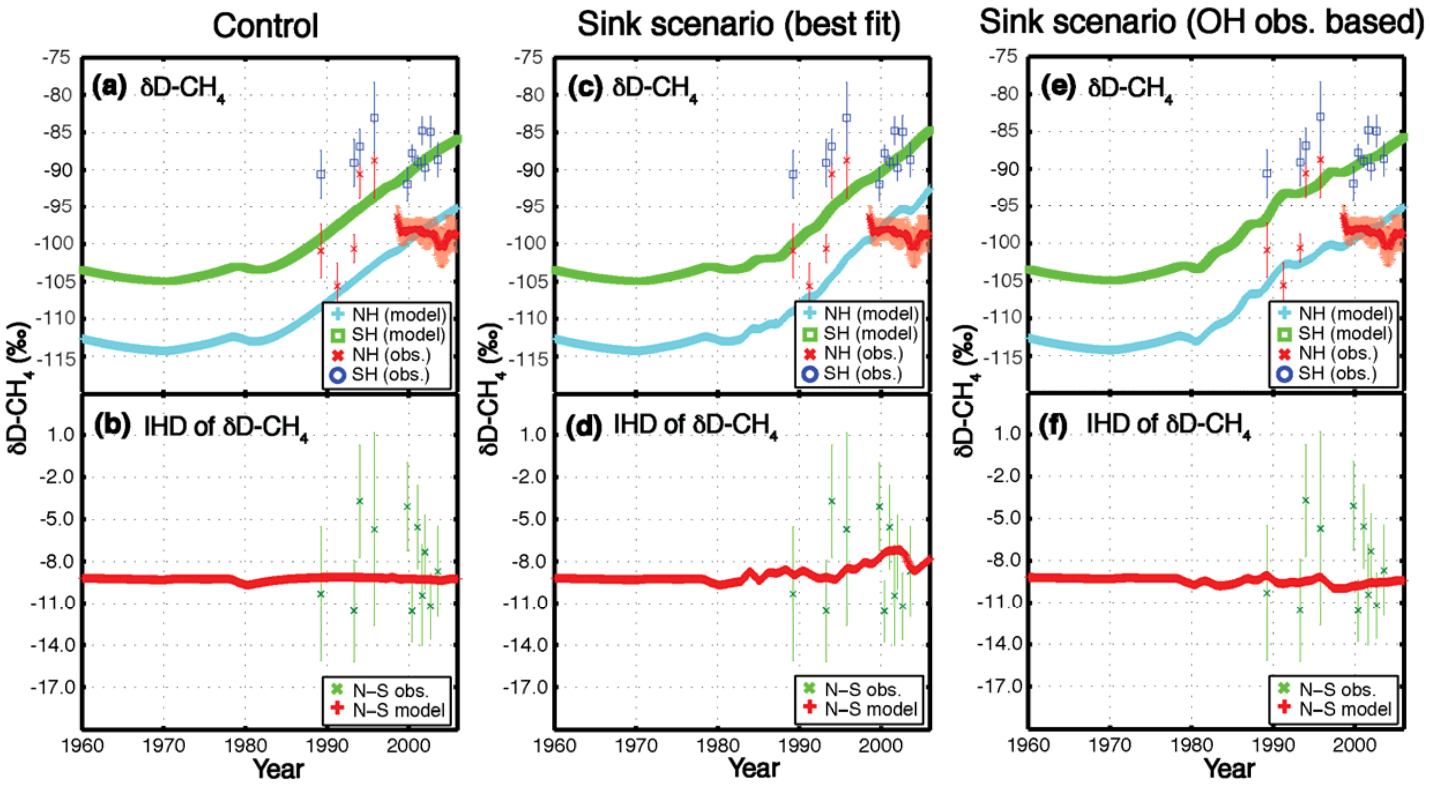

Fig. S16. Comparison of $\delta D\text{-}CH_4$ simulations between the control (scenario 1) and variable sink scenarios. In these scenarios, we tested whether the changes in sink processes could responsible for the CH_4 slow down by using the best-fit CH_4 lifetimes (see Fig. S13a) and OH lifetimes derived from a methyl chloroform inversion (see Fig. S13b). The model with the best-fit CH_4 lifetimes, which shows increasing OH level in the NH, could not improve the $\delta D\text{-}CH_4$ agreement between the model and observation (**c** and **d**). The $\delta D\text{-}CH_4$ agreement could be improved slightly (**e** and **f**) by applying the scenario with the OH–estimates derived from the methyl chloroform inversion, which shows decreasing OH levels in the NH. Error bars are 1 standard deviation (s.d.) based on the entire adjusted continental observations in a 12-month window centred at each monthly time step. For the Pacific voyage measurements, the error bars are 1 s.d. of the calculated monthly trends.

Table S1: Atmospheric CH_4 and its isotopic ratios measurements used for comparison in this work

Station Code (Network)	Location	Latitude	Longitude	Year of Data Used	Applied Measurements	Mean offset (ratio) with NWR	Mean offset (ratio) with BHD	References
				Northern Hemisphere sites				
NWR (UCI)	Niwot Ridge, Colorado	40˚N	105˚W	1989–2005 1989–2003 1998–2004	CH_4, $\delta^{13}C$-CH_4, δD-CH_4	Reference site		*Tyler et al*. (ref. 6); *Ajie et al*. (ref. 12); http://cdiac.ornl.gov/; data are updated here
MDO (UCI)	Montana de Oro, California	35˚N	121˚W	1996–2005 1996–2005 2000–2005	CH_4, $\delta^{13}C$-CH_4, δD-CH_4	1.0138 1.0009 1.0364		*Tyler et al*. (ref. 6); *Ajie et al*. (ref. 12); http://cdiac.ornl.gov/; data are updated here
POC* (UCI)	Pacific Ocean	10˚–40˚N	170˚E–110˚W	1997–2004 1997–2004 1999–2003	CH_4, $\delta^{13}C$-CH_4, δD-CH_4	0.9919 1.0002 0.9875		*Tyler et al*. (ref. 6); *Ajie et al*. (ref. 12); http://cdiac.ornl.gov/; data are updated here
POC* (NIWA)	Pacific Ocean	10˚–40˚N	170˚E–110˚W	1996–1998 1996–1998	CH_4, $\delta^{13}C$-CH_4,	0.9919 1.0002		*Bergamaschi et al*. (ref. 65); *Lowe et al*. (ref. 5,15)
UCI40N (UCI)		30˚–50˚N		1979–2005	CH_4	1.0063		*Simpson et al*. (refs. 3,13); http://cdiac.ornl.gov/
POC# (SIL)	Pacific Ocean	10˚–40˚N	~150˚W	1989–1995	δD-CH_4			*Quay et al*. (ref. 4).
				Southern Hemisphere sites				
BHD (NIWA)	Baring Head, New Zealand	41˚S	174˚E	1989–2005 1989–2005	CH_4, $\delta^{13}C$-CH_4,	Reference site		*Lowe et al*. (refs. 5,15); ftp://ftp.niwa.co.nz
AHT (NIWA)	Scott Base	77˚S	166˚E	1989–2005 1992–2004	CH_4, $\delta^{13}C$-CH_4,		0.9973 0.9997	*Lowe et al*. (ref. 5,15); ftp://ftp.niwa.co.nz
POC* (UCI)	Pacific Ocean	10˚–40˚S	170˚E–110˚W	1997–2004 1997–2004 1999–2003	CH_4, $\delta^{13}C$-CH_4, δD-CH_4		0.9964 0.9997	*Tyler et al*. (ref. 6); *Ajie et al*. (ref. 12); http://cdiac.ornl.gov/; data are updated here
POC* (NIWA)	Pacific Ocean	10˚–40˚S	170˚E–110˚W	1996–1998 1996–1998	CH_4, $\delta^{13}C$-CH_4,		0.9961 0.9997	*Bergamaschi et al*. (ref. 65); *Lowe et al*. (ref. 5,15)
UCI40S (UCI)		30˚–50˚S		1979–2005	CH_4		0.9945	*Simpson et al*. (ref. 3, 13); http://cdiac.ornl.gov/
POC# (SIL)	Pacific Ocean	10˚–40˚S	~150˚W	1989–1995	δD-CH_4			*Quay et al*. (ref. 4).

*UCIPOC and NIWAPOC are combined together, and then divided into NH (10–40˚N) and SH (10–40˚S) regions.
We used ship transect data, in the NH between 10 and 40˚N and in the SH between 10 and 40˚S. No offset ratio available because there is no period of overlap with the reference sites (NWR and BHD).

Table S2: Comparison of Measured and Simulated $\delta^{13}C$-CH_4

	$\delta^{13}C$ (‰) 1989–1993 (T_1)**			$\delta^{13}C$ (‰) 2001–2005 (T_2)**			*Difference of IHD (T_2 - T_1) (‰)	#Slope of IHD of $\delta^{13}C$ (‰ yr^{-1})
	NH	SH	IHD	NH	SH	IHD		
Observations:								
This study*	-47.40±0.07	-47.16±0.09	-0.24±0.11	-47.19±0.03	-47.09±0.01	-0.10±0.04	0.14±0.12	0.015±0.003
SIL	-47.51±0.11	-47.18±0.07	-0.33±0.13					
Model Simulations								
S1: Control	-47.46±0.01	-47.21±0.01	-0.25±0.01	-47.41±0.02	-47.15±0.01	-0.25±0.02	0.00±0.03	-0.000±0.000
S2: FF decrease	-47.42±0.02	-47.16±0.01	-0.26±0.02	-47.51±0.03	-47.18±0.04	-0.33±0.05	-0.07±0.05	-0.006±0.001
S3: Agr. decrease	-47.53±0.02	-47.29±0.03	-0.23±0.04	-47.21±0.05	-47.11±0.04	-0.09±0.06	0.14±0.07	0.011±0.002
Additional Model Sensitivity Simulations								
S4: FF+ others (ref. 8)	-47.43±0.02	-47.17±0.01	-0.25±0.02	-47.48±0.03	-47.18±0.03	-0.30±0.04	-0.05±0.04	-0.004±0.001
S5: S1 + neg. FF $\delta^{13}C$ trend	-47.59±0.01	-47.33±0.01	-0.26±0.01	-47.69±0.04	-47.42±0.03	-0.27±0.05	-0.01±0.05	-0.000±0.000
S6: S2 + neg. FF $\delta^{13}C$ trend	-47.55±0.01	-47.29±0.01	-0.27±0.01	-47.77±0.04	-47.44±0.05	-0.32±0.07	-0.06±0.07	-0.005±0.001
S7: Sink (best fit)	-47.47±0.01	-47.22±0.01	-0.25±0.02	-47.41±0.02	-47.14±0.01	-0.21±0.03	0.03±0.03	0.003±0.001
S8: Sink (obs.)	-47.39±0.01	-47.13±0.02	-0.26±0.02	-47.36±0.03	-47.16±0.02	-0.26±0.03	0.00±0.04	0.000±0.000

**Selected time period that T_1 is between 1989/1 (year/month) and 1993/12; T_2 is between 2001/1 and 2005/12; *The two $\delta^{13}C$ IHD's of this study in these two time periods (T_1 and T_2) were significantly different at a 95% confidence interval as assessed using Student's t test; # The error bars represent 95% confidence limits for the slopes during the time period between 1989/1 (year/month) and 2005/12

Table S3: CH_4 source inventory, $\delta^{13}C$ and δD signatures

Source	Source Input* (Tg yr^{-1})	Range of Estimates (Tg yr^{-1})	$\delta^{13}C$ (‰)	δD (‰)	Percentage of each source	
					NH	SH
Tundra	10[a]	5[e]–10[a]	-65[k]	-340[b]	98[e]	2[e]
Lakes (bogs, fens, and lakes)	40	38[f]–75[a]	-60[k]	-320[k]	85[e]	15[e]
Swamps and marshes	100	77[f] –106[a]	-60[k]	-320[k]	40[e]	60[e]
Agriculture (rice & livestock)	199[h]	105[d] –215[d]	-69[l]	-310[k]	84[e]	16[e]
Landfills	44[h]	35[d] –73[d]	-52[k]	-290[k]	86[e]	14[e]
Fossil fuels	76[h]	75[d] –110[d]	-38[k]	-160[f]	87[e]	13[e]
Biomass burning	35[h,i]	23[d] –55[d]	-23[j,k]	-225[f]	53[g]	47[g]
Termites	20[d]	16[f] –20[d]	-58[k]	-345[k]	55[e]	45[e]
Gas hydrates	10[a]	4[f] –10[a]	-52[k]	-205[c]	98[e]	2[e]
Total	559	378–674				

* Source input for control scenario in year 1980 (Tg CH_4 yr^{-1})
[a] *Tyler et al*. (ref. 6)
[b] *Steven and Wahlen* (ref. 66)
[c] *Matsumoto et al*. (ref. 67)
[d] *Prather et al.* (ref. 21)
[e] *Fung et al.* (ref. 7)
[f] *Whiticar and Schaefer* (ref. 56)
[g] *van der Werf et al.* (ref. 25)
[h] EDGAR-HYDE 1.4
[i] We added 10 Tg yr^{-1} to the biomass burning source, to improve agreement with ice core observation of $\delta^{13}C$ during 1800–1900.
[j] We assumed 70% of the biomass burning source is from C3 plants and 30% is from C4 plants (ref. 68)
[k] Modified isotope values are taken from *Tyler et al*. (ref. 6)
[l] Based on *Cicerone and Oremland* (ref. 55), where the range of the agricultural carbon isotope values is between -45 and -76‰.

Table S4: Characteristics and results of model sensitivity and Monte Carlo simulations

Sensitivity Test	^{13}C Kinetic isotopic fractionation (‰)	Exchange rate (Month)	δ^{13}C-CH_4 signature (‰)		IHD of δ^{13}C ($T_2 - T_1$)* (‰)	#Slope of IHD of δ^{13}C (‰ yr^{-1})
			Fossil Fuel	Agriculture		
Observations					0.14	0.015
			Control			
S-01	5.4	12	-38	-69	0.00	-0.000
ST-01	7.7	12	-38	-69	-0.00	-0.000
ST-02	[3.9 7.7] [a]	[6 18] [a]	[-44 -38] [a]	[-69 -60] [a]	-0.00±0.00	-0.000±0.000
		Fossil Fuel Scenarios and Sensitivity Tests				
S-02	5.4	12	-38	-69	-0.07	-0.006
ST-03	3.9	12	-38	-69	-0.08	-0.007
ST-04	7.7	12	-38	-69	-0.06	-0.005
ST-05	5.4	12	-44	-69	-0.03	-0.003
ST-06	5.4	6	-38	-69	-0.04	-0.003
ST-07	5.4	18	-38	-69	-0.13	-0.008
ST-08	5.4	[6 18] [a]	-38	-69	-0.07±0.02	-0.006±0.002
ST-09	5.4	12	-38	[-69 -60] [a]	-0.05±0.01	-0.004±0.001
ST-10	5.4	12	[-44 -38] [a]	[-69 -60] [a]	-0.04±0.01	-0.004±0.001
ST-11	5.4	[6 18] [a]	[-44 -38] [a]	[-69 -60] [a]	-0.04±0.02	-0.004±0.001
ST-12	7.7	[6 18] [a]	[-44 -38] [a]	[-69 -60] [a]	-0.03±0.02	-0.003±0.001
ST-13	[3.9 7.7] [a]	[6 18] [a]	[-44 -38] [a]	[-69 -60] [a]	-0.04±0.02	-0.004±0.001
		Agriculture Scenarios and Sensitivity Tests				
S-03	5.4	12	-38	-69	0.14	0.011
ST-14	3.9	12	-38	-69	0.13	0.010
ST-15	7.7	12	-38	-69	0.15	0.012
ST-16	5.4	12	-44	-69	0.14	0.011
ST-17	5.4	12	-38	-60	0.10	0.008
ST-18	5.4	6	-38	-69	0.07	0.006
ST-19	5.4	18	-38	-69	0.20	0.016
ST-20	5.4	[6 18] [a]	-38	-69	0.14±0.04	0.011±0.003
ST-21	5.4	12	[-44 -38] [a]	-69	0.12±0.01	0.009±0.001
ST-22	5.4	12	[-44 -38] [a]	[-69 -60] [a]	0.12±0.01	0.009±0.001
ST-23	5.4	[6 18] [a]	[-44 -38] [a]	[-69 -60] [a]	0.11±0.03	0.009±0.003
ST-24	7.7	[6 18] [a]	[-44 -38] [a]	[-69 -60] [a]	0.12±0.04	0.010±0.003
ST-25	[3.9 7.7] [a]	[6 18] [a]	[-44 -38] [a]	[-69 -60] [a]	0.11±0.03	0.009±0.003

* Selected time period that T_1 is between 1989/1 (year/month) and 1993/12; T_2 is between 2001/1 and 2005/12. # Time period between 1989/1 and 2005/12. [a] run Monte Carlo simulation 1000 times. Error bars are 1 s.d. of the calculated mean of model results (n=1000).